University of Reading

Thermal acclimation of stem respiration implies a weaker carbon-climate feedback

Article

Accepted Version

Zhang, H. ORCID: https://orcid.org/0009-0008-9231-2939, Wang, H. ORCID: https://orcid.org/0000-0003-2482-1818, Wright, I. J. ORCID: https://orcid.org/0000-0001-8338-9143, Prentice, I. C. ORCID: https://orcid.org/0000-0002-1296-6764, Harrison, S. P. ORCID: https://orcid.org/0000-0001-5687-1903, Smith, N. G. ORCID: https://orcid.org/0000-0001-7048-4387, Westerband, A. C. ORCID: https://orcid.org/0000-0003-4065-9689, Rowland, L. ORCID: https://orcid.org/0000-0002-0774-3216, Plavcová, L. ORCID: https://orcid.org/0000-0002-3395-4463, Morris, H. ORCID: https://orcid.org/0000-0002-7548-0796, Reich, P. B. ORCID: https://orcid.org/0000-0003-4424-662X, Jansen, S. ORCID: https://orcid.org/0000-0002-4476-5334, Keenan, T. ORCID: https://orcid.org/0000-0002-3347-0258 and Nguyen, N. B. ORCID: https://orcid.org/0000-0002-4634-8390 (2025) Thermal acclimation of stem respiration implies a weaker carbon-climate feedback. Science, 388 (6750). pp. 984-988. ISSN 1095-9203 doi: 10.1126/science.adr9978 Available at https://centaur.reading.ac.uk/123139/

It is advisable to refer to the publisher's version if you intend to cite from the work. See Guidance on citing.

University of Reading

To link to this article DOI: http://dx.doi.org/10.1126/science.adr9978

Publisher: American Association for the Advancement of Science (AAAS)

All outputs in CentAUR are protected by Intellectual Property Rights law, including copyright law. Copyright and IPR is retained by the creators or other copyright holders. Terms and conditions for use of this material are defined in the End User Agreement.

www.reading.ac.uk/centaur

CentAUR

Central Archive at the University of Reading

Reading's research outputs online

Thermal acclimation of stem respiration implies a weaker carbon-climate feedback

Authors: Han Zhang[1], Han Wang[1 *], Ian J. Wright[2,3,4], I. Colin Prentice[1,5], Sandy P. Harrison[1,6], Nicholas G. Smith[7], Andrea C. Westerband[2], Lucy Rowland[8], Lenka Plavcová[9], Hugh Morris[10], Peter B. Reich[2,11,12], Steven Jansen[13], Trevor Keenan[14,15], Ngoc Bao Nguyen[14]

Affiliations:

[1] Department of Earth System Science, Ministry of Education Key Laboratory for Earth System Modeling, Institute for Global Change Studies, Tsinghua University, Beijing, China;

[2] Hawkesbury Institute for the Environment, Western Sydney University, Sydney, Australia;

[3] School of Natural Sciences, Macquarie University, NSW 2109, Australia;

[4] ARC Centre for Plant Success in Nature & Agriculture, Western Sydney University, Richmond, NSW 2753, Australia;

[5] Department of Life Sciences, Imperial College London, Silwood Park Campus, Buckhurst Road, Ascot SL5 7PY, United Kingdom;

[6] School of Archaeology, Geography and Environmental Science (SAGES), University of Reading, Reading RG6 6AH, United Kingdom;

[7] Department of Biological Sciences, Texas Tech University, Lubbock, Texas, USA;

[8] Faculty of Environment, Science and Economy, University of Exeter, Exeter, EX4 4RJ, United Kingdom;

[9] Faculty of Forestry and Wood Sciences, Czech University of Life Sciences, Prague, Czech Republic;

[10] Department of Integrated Land Management, SRUC, Barony, Parkgate, Dumfries DG1 3NE, UK;

[11] Institute for Global Change Biology and School for Environment and Sustainability, University of Michigan, Ann Arbor, Michigan, USA;

[12] Department of Forest Resources, University of Minnesota, St. Paul, Minnesota, USA;

[13] Institute of Botany, Ulm University, Ulm, Germany;

[14] Department of Environmental Science, Policy and Management, University of California Berkeley, Berkeley, CA, USA;

[15] Climate and Ecosystem Sciences Division, Lawrence Berkeley National Laboratory, Berkeley, CA, USA;

*Corresponding author. Email: wang_han@tsinghua.edu.cn

Abstract: The efflux of CO_2 from woody stems, a proxy for stem respiration, is a critical carbon flux from ecosystems to atmosphere, increasing with temperature on short timescales. However, plants acclimate their respiratory response to temperature on longer timescales, potentially weakening the carbon-climate feedback. The magnitude of this acclimation is uncertain despite its importance for predicting future climate change. We develop an optimality-based theory dynamically linking stem respiration with leaf water supply to predict its thermal acclimation. We show the theory accurately reproduces observations of spatial and seasonal change. We estimate stem respiration emitting 18.8±5.9 PgC annually at present. Incorporating thermal acclimation reduces projected land ecosystem carbon emissions by 7.4 to 16.5 PgC by 2100, about 24% to 46% of projected stem respiration without acclimation.

Main text

Plant respiration represents about half of the annual carbon flux globally from terrestrial ecosystems to the atmosphere, approximately six times more than anthropogenic carbon emissions (*1, 2*). The contribution of respiration by stems is not well quantified (Guan et al., 2006; Malhi et al., 2009; Campioli et al., 2016), but current models estimate it as around a quarter of total plant respiration (fig. S12). Plants respire their photosynthetic products to support physiological processes and growth (*3, 4*). As an enzyme-mediated process, respiration increases nearly exponentially with increasing temperature on time frames of minutes to hours (*5*). Additional respiratory carbon release is thus widely expected in a warming world, leading to more warming (*6, 7*).

In principle, plant respiration is controlled by substrate availability, oxygen supply and the demand for respiratory products. Plants modulate their respiratory response to temperature on timescales of weeks to years due to changes in these driving forces (*8-10*). This behaviour could weaken the positive feedback between the climate warming and carbon emissions from plants. Plants exposed to warmer conditions show a reduced respiration rate at a standardized measurement temperature, and/or a decreased sensitivity to temperature (indicated by a smaller increase in respiratory rate per unit increase in temperature over the short term) compared to plants that have experienced cooler temperatures (*8-13*). These adjustments are called 'thermal acclimation'. The more pronounced the thermal acclimation of respiration globally, the weaker the positive feedback between climate warming and carbon emissions.

The mechanisms and magnitude of thermal acclimation are still unclear. This is particularly true for stem respiration. Empirical evidence shows that stem respiration scales with nitrogen concentration similarly to leaves and roots, reflecting its enzyme requirements (*14, 15*). However, the nature of thermal acclimation may differ between tissues. Leaves coordinate their respiratory acclimation with photosynthetic acclimation and have multiple mechanisms for thermal and physiological regulation (refs). This is unlikely appliable to stems and roots, which however probably have higher thermal inertia than leaves (*16, 17*). There have been a number of studies on the environmental controls of stem respiration, but no overarching principle has emerged (*18-23*). The lack of a theoretical basis has precluded any global analysis of the impact of the thermal acclimation of stem respiration.

The representation of respiration in Earth System Models (ESMs) is simplistic and largely untested. Many ESMs do not implement time-dependent acclimation of plant respiration rates to warming (*24, 25*). Models that do consider acclimation use empirical approaches and either ignore stem respiration or assume that stems acclimate in the same way as leaves (*26-29*), presumably due to the paucity of information about stem respiration. Improved understanding of the magnitude of stem respiration and its acclimation is needed for reliable predictions of the global carbon-climate feedback (*30*).

Eco-evolutionary optimality (EEO) principles have been shown to provide parameter-sparse predictions of many different plant processes (*11, 13, 31-33*). EEO hypotheses identify trade-offs between plant resource demand and acquisition that can be expressed mathematically (*31*). The previous success of EEO in predicting plant eco-physiological processes suggests this approach as also useful to investigate the magnitude of thermal acclimation in stems. This study addresses the following two questions: (1) Is thermal acclimation of stem respiration effectively described by EEO theory? (2) How does thermal acclimation affect the global carbon cycle? We first propose an EEO-based model for the thermal sensitivity of stem respiration, which we test both spatially, using a global dataset, and temporally, using seasonal measurements and a warming experiment. We then apply the resulting model to test the impact of thermal acclimation on the global carbon cycle under future climate.

Theoretical background

Under the assumption that a primary function of sapwood is maintaining the hydraulic continuum as determined by the canopy water demand, we assumed that the cost of doing so – whole-plant stem respiration – is proportional to transpiration from the canopy on a timescale of days to weeks (SI section 2.1). This coupling ensures that total stem respiration, including both maintenance and growth components, is neither more (which would result in non-productive carbon consumption) nor less (which would threaten hydraulic integrity) than that required to support the stem hydraulic continuum. Although long-distance water transport through the xylem is largely driven passively, maintenance of the hydraulic continuum is effectively used here as a proxy for associated energy-requiring processes, including the maintenance of stem water storage capacity, new xylem production, defense and resilience to disturbance, and the maintenance of stem water potential (SI section 1.4) (*34-38*). We combine this hypothesis with physical principles influencing the manner in which respiration and transpiration are coupled and use this relationship to predict the spatial and temporal thermal acclimation of stem respiration. First, we assume that whole-plant stem respiration (R_s, nmol C s^{-1}) is proportional to canopy transpiration (E, nmol H_2O s^{-1}) with a cost factor representing the respiration rate required to maintain a unit of transpiration rate (*39*). In principle, this cost factor should be influenced by temperature: water has a reduced dynamic viscosity as temperature increases, meaning there is less hydraulic resistance to water transport to the leaves, and thus the cost incurred for supporting a given transpiration rate would be lower. Given that R_s is a product of mass-based respiration rate over time (r_s, nmol C g^{-1} s^{-1}) and total sapwood mass (M_s, g C), we expect that r_s and M_s also co-vary with E and the respiration cost of transpiration. At a global scale, where spatial variation in both r_s and M_s is large, we assume that r_s and M_s track variation in the cost factor and E, respectively (Eq. 20). Therefore, the thermal response of the cost factor as largely determined by the hydraulic resistance and xylem sap viscosity is the primary control of the variation in r_s along geographic temperature gradients. For temporal changes at a weekly scale, where the change in M_s is small compared

to changes in transpiration, we expect only r_s to be coordinated with temporal variation in both E and the cost factor (Eq. 19). Therefore, the response of r_s to temperature that emerges over time dominated by acclimation should be mathematically the same as that emerging across space dominated by adaptation.

To generate empirically testable predictions for the adjustment of stem respiration to temperature, we calculated r_s at growth temperature ($r_{s,gt}$, nmol C g^{-1} s^{-1}) and r_s at a standard temperature of 25°C (r_{s25}, nmol C g^{-1} s^{-1}) applying a constant Q_{10} temperature coefficient. $r_{s,gt}$ provides a measure of respiration rate under temperature conditions experienced by plants growing under natural conditions, while r_{s25} allows for a standardized comparison of respiratory capacity (and associated investment in mitochondrial proteins) across sites and species (*40*). Our model specifically predicts that $r_{s,gt}$ acclimates to increasing temperature by −2.3% K^{-1} (Fig. 1B, Eq. 22) due to the decline in the viscosity of water. A steeper decline, of −10.1% K^{-1}, is expected for r_{s25} adjusting to temperature (Fig. 1A, Eq. 20) because of the greater catalytic rates of respiratory enzymes at higher temperatures. The trend in the thermal response when considering acclimation is opposite to the instantaneous response due to enzyme kinetics (+7.9% K^{-1}) (Eq. 7), which means that warming in the short term will increase respiration steeply and exponentially. Therefore, with acclimation to warming in the long term, respiration at a given temperature (r_{s25}) is reduced, reflecting reduction in respiratory capacity.

We evaluated the thermal response of stem respiration via empirical analyses using a new Global Stem Respiration Dataset (GSRD) (fig. S1 and table S1-2). GSRD includes 5 species measured from a warming experiment and 187 species sampled at 69 sites spanning all climate zones, which consist of 4546 measurements from 64 sites directly taken in the field on trunks, 81 measurements from 4 sites made on cut branches in the laboratory, and 4155 seasonal measurements from one site.

Results

A linear regression of r_{s25} against the mean value of the excess temperature above 5°C (T_5) showed a strong negative response to higher temperatures across all sites globally: r_{s25} decreased by 9.8±0.3% K^{-1} with warmer temperatures, statistically indistinguishable with our theoretical prediction (10.1% K^{-1}) (Fig. 1A, Table 1 and table S3). Measurements made in the field and in the laboratory showed a similar thermal response for r_{s25} (field measurements: –10.1±0.3% K^{-1}; laboratory measurements: –11.0±3.3% K^{-1}). The absolute values of the laboratory measurements (2.97±1.94 nmol CO_2 g^{-1} s^{-1}) were generally larger than that of the field measurements (0.87±0.14 nmol CO_2 g^{-1} s^{-1}), possibly because some CO_2 dissolved and transported into upward sap flow in the field and limitations on CO_2 diffusion from bark were removed in the laboratory (table S4). A higher proportion of living cells in smaller branches might also explains (Cavaleri et al., 2006). Comparisons using site-mean values, to minimize the potential impact of over-representation of individual sites with much larger sample sizes, showed that r_{s25} decreased by 8.1±1.8% K^{-1} with warmer temperatures (fig. S2 and table S5). We also tested whether using the different thermal sensitivity to calculate r_{s25} impacted the temperature response, by restricting our analyses to sites where respiration rate was directly measured at a temperature of 25±1 °C; these data showed a similar thermal response in r_{s25} (site-mean: 10.1±3.8% K^{-1}, all individuals: 15.5±0.7% K^{-1}) (fig. S3 and table S6). Thus, the observed response of r_{s25} against T_5, considered multiple ways, was in the range of ca. −8% K^{-1} to −15% K^{-1}. Under typical growing conditions, both observations and theory showed a significant negative

response of $r_{s.gt}$ to temperature (data: −1.5±0.3% K^{-1}, theory: −2.3% K^{-1}), opposite in trend from that expected from enzyme kinetics alone (Fig. 1B and Table 1).

While the global patterns are consistent with an acclimation response to temperature, they may also reflect species replacement along geographic temperature gradients (fig. S4). However, measurements of seasonal variation and a warming experiment are consistent with our theoretical predictions. A single boreal site provided continuous data on r_s of three species throughout the growing season. We estimated daily transpiration (nmol m^{-2} s^{-1}) with an EEO-based Penman-Monteith model accounting canopy stomatal regulation driven by radiation, temperature, vapor pressure deficit, atmospheric pressure and leaf area index (*41*). The best predictions of the temporal variation in r_{s25}, indicated by variance inflation factor, root mean square error and R^2, were given by a 6-day time window for temperature and a 13-day period for transpiration, though alternative periods around one to two weeks generate similar predictions (fig. S5, table S7). A multiple regression showed that r_{s25} declines with acclimated temperature by 10.6±0.5% K^{-1} and increases almost proportionally to transpiration (103.8±1.8%), consistent with the theoretical predictions (temperature: −10.1% K^{-1}, transpiration: 100 %, Fig. 2). When evaluating at the acclimated temperature, $r_{s.gt}$ also showed significant responses to temperature (−4.7±0.5% K^{-1}) and to transpiration (111.7±1.8%), stronger than the theoretical ones (temperature: −2.3% K^{-1}, transpiration: 100%) (fig. S6). The small differences between the theoretical and empirical values likely reflect uncertainties in the two predictors or the influence of other potential explanatory variables such as soil moisture (see below). The five species measured in the warming experiment showed a consistent decrease in r_{s25} of 10.6±1.6% K^{-1}, close to our theoretical prediction of 10.1% (Fig. 3). Individual species show similar trends (Fig. 3 and table S8). The four *Pinus* species in this experiment showed a somewhat stronger thermal acclimation response than *Pinus* species in the global analysis (−8.4±0.4% K^{-1}), possibly reflecting differences in the temperature range sampled (fig. S4 and table S9).

Based on the agreement between theory and observations, we developed a simple model to estimate the global carbon flux from stem respiration and its contribution to the global carbon cycle (SI section 3.2.1). In this model, total stem respiration rate per unit land area is predicted as the product of sapwood mass and stem respiration rate under growing temperature ($r_{s.gt}$), on an annual time-step. Sapwood mass is estimated from total above-ground stem biomass and allometric equations with five parameters defining shape of the stem and sapwood depth (Eq. 35) (*42, 43*). We simulated $r_{s.gt}$ with a single global parameter (table S10) and T_5 to represent the annual growth thermal environment for woody species. The model predicts an annual carbon release by stem respiration globally in 2010 of 18.8±5.9 Pg C, about 15% of global GPP (Fig. 4A) (*44, 45*). This is consistent with the average from TRENDY model outputs (fig. S7). Modelled stem respiration from forests alone (excluding shrublands and savannas) is 10.5±3.2 Pg C, somewhat higher than a previous empirical estimate (*22*)(6.7±0.5 Pg C) with the difference presumably reflecting different methods of estimation. Global variation in stem respiration was largely controlled by total stem biomass: regions with higher biomass had higher respiration. The highest stem respiration occurred in tropical forests and in the humid temperate forests of eastern North America, eastern Asia and Europe.

We applied this modelling scheme using different climate change scenarios to assess the influence of thermal acclimation on the carbon flux from stem respiration over the 21st century. The results showed

that implementing thermal acclimation led to a reduction in stem respiration of 24% and 46% by 2100, and reduced predicted land ecosystem carbon emissions by 7.4 and 16.5 Pg C, under the smallest (SSP126) and largest (SSP585) warming scenarios, respectively (Fig. 4B). Some Land Surface Models, including CLM5, CABLE and QUINCY, consider the thermal acclimation of stem respiration but treat it identically to leaf respiration (*24, 27, 29, 40*). In those models, r_{s25} is predicted to decrease with temperature by 1.83 % K^{-1}, an order of magnitude less than that shown by our empirical analyses. This underestimation of the thermal acclimation of stem respiration led to a higher carbon emission from terrestrial ecosystems, resulting in an overestimation of 5.4 and 13.9 PgC in 2100 under the SSP126 and SSP585 scenarios, respectively (SI section 3.2.5).

Discussion and conclusion

We considered several sources of uncertainty inherent in stem respiration observations from assumptions about mean stem diameter values and the allometric equation for deriving mass-based estimates of respiration from stem surface area-based measurements (SI section 1.1.4). Stem size shows a further significant negative effect on stem respiration (tables S13), probably reflecting the lower proportion of living cells from allometric constraints and likely contributing to the difference between lab and field observations. Uneven geographic coverage of observations, with relatively few sites from the tropics and southern hemisphere, may have introduced further biases. Nevertheless, the trends are consistent across the range of temperatures, including boreal and tropical sites. A remaining uncertainty concerns the use of stem CO_2 efflux as a proxy for stem respiration, since there can be other processes affecting stem CO_2 efflux such as CO_2 refixation and dissolution in xylem sap (*46-48*). Nevertheless, the congruence of the results across different sources and subsets of the data (Figs. 1-3, figs. S2-4, 9, Table 1 and tables S3, 5-6, 9, 14) and the similarity between the observed and predicted relationships suggests that our conclusions about the thermal response of stem respiration are robust. Data limitations preclude further analysis of the sensitivity of respiration to other environmental factors, such as soil moisture (*21, 49*) or CO_2 concentration. However, we note that vapor pressure deficit had a positive influence on r_{s25}, in line with our theoretical prediction (SI section 2.2, figs. S10-11 and table S15). Q_{10} temperature coefficient might also acclimate to warming and modify the estimates on r_{s25} and $r_{s.gt}$ *(9)*. However, our sensitivity analysis by applying a range of Q_{10} values (table S11) and analysis without temperature standardization (fig. S3 and table S6) show that variation in Q_{10} has minor influence on the agreement between theoretical prediction and empirical observations. Overall, despite the different magnitudes shown in various data analyses (Fig. 1B, figs. S6 and S8), stem respiration – as our hypothesis predicts – appears to show a much stronger thermal acclimation than leaf respiration, which shows a weak but positive response to warming (*13*). This disparity potentially comes from their different driving processes and thermal conditions. Leaf respiration is suggested to track the maximum capacity of carboxylation *(11, 13)*. The acclimated carboxylation capacity increases with temperature compensating the enhanced photorespiration at a warmer condition, consequently implies a positive thermal response in leaf respiratory acclimation. This is probably not the case for woody tissues. Furthermore, leaves are more likely to be sun-exposed and do not have the insulating properties of bark tissue (*50, 51*). Experimental studies will be needed to reveal the mechanisms controlling the acclimation of stem and leaf respiration.

We have demonstrated that the application of EEO principles provides a simple way to predict stem

respiration and its thermal acclimation, consistent with empirical evidence. This approach could and should be implemented in ESMs. The acclimation response to growth temperature in stem respiration is much stronger than that in leaf respiration. This suggests a potential for enhanced carbon use efficiency in a warming world, a subject still considerably debated (*52-54*). Enhanced carbon use efficiency would, in turn, substantially weaken the expected positive climate-carbon feedback, enhancing the degree to which ecosystems globally slow the rate of climate change.

References and Notes

1. P. Ciais *et al.*, in *Climate Change 2013: The Physical Science Basis*. (Cambridge University Press, 2014), pp. 465-570.
2. P. Friedlingstein *et al.*, Global Carbon Budget 2023. *Earth Syst Sci Data* **15**, 5301-5369 (2023).
3. J. S. Amthor, The McCree-de Wit-Penning de Vries-Thornley respiration paradigms: 30 years later. *Annals of Botany* **86**, 1-20 (2000).
4. F. d. Vries, The cost of maintenance processes in plant cells. *Annals of Botany* **39**, 77-92 (1975).
5. M. A. Heskel *et al.*, Convergence in the temperature response of leaf respiration across biomes and plant functional types. *P Natl Acad Sci USA* **113**, 3832-3837 (2016).
6. P. M. Cox, R. A. Betts, C. D. Jones, S. A. Spall, I. J. Totterdell, Acceleration of global warming due to carbon-cycle feedbacks in a coupled climate model. *Nature* **408**, 184-187 (2000).
7. C. Huntingford *et al.*, Simulated resilience of tropical rainforests to CO_2-induced climate change. *Nat Geosci* **6**, 268-273 (2013).
8. O. K. Atkin, M. G. Tjoelker, Thermal acclimation and the dynamic response of plant respiration to temperature. *Trends Plant Sci* **8**, 343-351 (2003).
9. K. Y. Crous, J. Uddling, M. G. De Kauwe, Temperature responses of photosynthesis and respiration in evergreen trees from boreal to tropical latitudes. *New Phytologist* **234**, 353-374 (2022).
10. P. B. Reich *et al.*, Boreal and temperate trees show strong acclimation of respiration to warming. *Nature* **531**, 633-+ (2016).
11. Y. H. Ren *et al.*, Reduced global plant respiration due to the acclimation of leaf dark respiration coupled with photosynthesis. *New Phytologist* **241**, 578-591 (2024).
12. N. G. Smith, G. Y. Li, J. S. Dukes, Short-term thermal acclimation of dark respiration is greater in non-photosynthetic than in photosynthetic tissues. *Aob Plants* **11**, plz064 (2019).
13. H. Wang *et al.*, Acclimation of leaf respiration consistent with optimal photosynthetic capacity. *Global Change Biology* **26**, 2573-2583 (2020).
14. P. B. Reich *et al.*, Scaling of respiration to nitrogen in leaves, stems and roots of higher land plants. *Ecol Lett* **11**, 793-801 (2008).
15. A. C. Westerband *et al.*, Nitrogen concentration and physical properties are key drivers of woody tissue respiration. *Annals of Botany* **129**, 633-646 (2022).
16. S. T. Michaletz *et al.*, The energetic and carbon economic origins of leaf thermoregulation. *Nat Plants* **2**, 16129 (2016).
17. B. C. Posch *et al.*, Intensive leaf cooling promotes tree survival during a record heatwave. *P Natl Acad Sci USA* **121**, (2024).
18. J. Q. Chambers *et al.*, Respiration from a tropical forest ecosystem: Partitioning of sources and low carbon use efficiency. *Ecol Appl* **14**, 72-88 (2004).
19. D. Gansert, K. Backes, T. Ozaki, Y. Kakubari, Seasonal variation of branch respiration of a treeline forming (*Betula*

ermanii Cham.) and a montane (*Fagus crenata* Blume) deciduous broad-leaved tree species on Mt. Fuji, Japan. *Flora* **197**, 186-202 (2002).

20. M. B. Lavigne, M. G. Ryan, Growth and maintenance respiration rates of aspen, black spruce and jack pine stems at northern and southern BOREAS sites. *Tree Physiology* **17**, 543-551 (1997).
21. L. Rowland *et al.*, Drought stress and tree size determine stem CO_2 efflux in a tropical forest. *New Phytologist* **218**, 1393-1405 (2018).
22. J. Y. Yang, Y. J. He, D. P. Aubrey, Q. L. Zhuang, R. O. Teskey, Global patterns and predictors of stem CO_2 efflux in forest ecosystems. *Global Change Biology* **22**, 1433-1444 (2016).
23. A. Zach, V. Horna, C. Leuschner, Diverging temperature response of tree stem CO_2 release under dry and wet season conditions in a tropical montane moist forest. *Trees-Structure and Function* **24**, 285-296 (2010).
24. G. Krinner *et al.*, A dynamic global vegetation model for studies of the coupled atmosphere-biosphere system. *Global Biogeochem Cy* **19**, GB1015 (2005).
25. G. Y. Niu *et al.*, The community Noah land surface model with multiparameterization options (Noah-MP): 1. Model description and evaluation with local-scale measurements. *Journal of Geophysical Research-Atmospheres* **116**, D12109 (2011).
26. D. B. Clark *et al.*, The Joint UK Land Environment Simulator (JULES), model description - Part 2: Carbon fluxes and vegetation dynamics. *Geosci Model Dev* **4**, 701-722 (2011).
27. V. Haverd *et al.*, A new version of the CABLE land surface model (Subversion revision r4601) incorporating land use and land cover change, woody vegetation demography, and a novel optimisation-based approach to plant coordination of photosynthesis. *Geosci Model Dev* **11**, 2995-3026 (2018).
28. D. M. Lawrence *et al.*, The Community Land Model Version 5: Description of New Features, Benchmarking, and Impact of Forcing Uncertainty. *J Adv Model Earth Sy* **11**, 4245-4287 (2019).
29. T. Thum *et al.*, A new model of the coupled carbon, nitrogen, and phosphorus cycles in the terrestrial biosphere (QUINCY v1.0; revision 1996). *Geosci Model Dev* **12**, 4781-4802 (2019).
30. D. L. Lombardozzi, G. B. Bonan, N. G. Smith, J. S. Dukes, R. A. Fisher, Temperature acclimation of photosynthesis and respiration: A key uncertainty in the carbon cycle-climate feedback. *Geophysical Research Letters* **42**, 8624-8631 (2015).
31. S. P. Harrison *et al.*, Eco-evolutionary optimality as a means to improve vegetation and land-surface models. *New Phytologist* **231**, 2125-2141 (2021).
32. A. Lavergne *et al.*, Historical changes in the stomatal limitation of photosynthesis: empirical support for an optimality principle. *New Phytologist* **225**, 2484-2497 (2020).
33. H. Wang *et al.*, Towards a universal model for carbon dioxide uptake by plants. *Nat Plants* **3**, 734-741 (2017).
34. A. Gauthey *et al.*, Mechanisms of xylem hydraulic recovery after drought in Eucalyptus saligna. *Plant Cell and Environment* **45**, 1216-1228 (2022).
35. S. Martorell, A. Diaz-Espejo, H. Medrano, M. C. Ball, B. Choat, Rapid hydraulic recovery in Eucalyptus pauciflora after drought: linkages between stem hydraulics and leaf gas exchange. *Plant Cell and Environment* **37**, 617-626 (2014).
36. H. Morris *et al.*, A global analysis of parenchyma tissue fractions in secondary xylem of seed plants. *New Phytologist* **209**, 1553-1565 (2016).
37. M. Tomasella, E. Petrussa, F. Petruzzellis, A. Nardini, V. Casolo, The Possible Role of Non-Structural Carbohydrates in the Regulation of Tree Hydraulics. *Int J Mol Sci* **21**, 144 (2020).
38. M. J. B. Zeppel *et al.*, Embolism recovery strategies and nocturnal water loss across species influenced by

biogeographic origin. *Ecol Evol* **9**, 5348-5361 (2019).
39. I. C. Prentice, N. Dong, S. M. Gleason, V. Maire, I. J. Wright, Balancing the costs of carbon gain and water transport: testing a new theoretical framework for plant functional ecology. *Ecol Lett* **17**, 82-91 (2014).
40. O. K. Atkin *et al.*, Global variability in leaf respiration in relation to climate, plant functional types and leaf traits. *New Phytologist* **206**, 614-636 (2015).
41. S. Tan *et al.*, Towards a universal evapotranspiration model based on optimality principles. *Agricultural and Forest Meteorology* **336**, 109478 (2023).
42. M. Santoro *et al.*, The global forest above-ground biomass pool for 2010 estimated from high-resolution satellite observations. *Earth Syst Sci Data* **13**, 3927-3950 (2021).
43. M. Thurner *et al.*, Sapwood biomass carbon in northern boreal and temperate forests. *Global Ecol Biogeogr* **28**, 640-660 (2019).
44. C. Huntingford *et al.*, Implications of improved representations of plant respiration in a changing climate. *Nat Commun* **8**, 1602 (2017).
45. M. Jung *et al.*, Global patterns of land-atmosphere fluxes of carbon dioxide, latent heat, and sensible heat derived from eddy covariance, satellite, and meteorological observations. *Journal of Geophysical Research-Biogeosciences* **116**, G00J07 (2011).
46. R. L. Salomón, L. De Roo, J. Oleksyn, D. J. W. De Pauw, K. Steppe, TReSpire - a biophysical TRee Stem respiration model. *New Phytologist* **225**, 2214-2230 (2020).
47. R. L. Salomón *et al.*, The quandary of sources and sinks of CO_2 efflux in tree stems-new insights and future directions. *Tree Physiology* **44**, tpad157 (2024).
48. R. O. Teskey, A. Saveyn, K. Steppe, M. A. McGuire, Origin, fate and significance of CO_2 in tree stems. *New Phytologist* **177**, 17-32 (2008).
49. C. W. Huang *et al.*, The effect of plant water storage on water fluxes within the coupled soil-plant system. *New Phytologist* **213**, 1093-1106 (2017).
50. N. L. Harris, C. A. S. Hall, A. E. Lugo, Estimates of species- and ecosystem-level respiration of woody stems along an elevational gradient in the Luquillo Mountains, Puerto Rico. *Ecol Model* **216**, 253-264 (2008).
51. Q. Yang, Ming Xu, Yonggang Chi and Yunpu Zheng., Relationship between stem CO_2 efflux and stem temperature at different measuring depths in Pinus massoniana trees. *Acta Ecologica Sinica* **36**, 229-235 (2016).
52. M. Campioli, Vicca, S., Luyssaert, S. et al., Biomass production efficiency controlled by management in temperate and boreal ecosystems. *Nat Geosci* **8**, 843–846 (2015).
53. A. Collalti *et al.*, Forest production efficiency increases with growth temperature. *Nat Commun* **11**, 5322 (2020).
54. S. Manzoni *et al.*, Reviews and syntheses: Carbon use efficiency from organisms to ecosystems - definitions, theories, and empirical evidence. *Biogeosciences* **15**, 5929-5949 (2018).
55. H. Zhang *et al.*, Global Stem Respiration Dataset (GSRD), version 1, Science Data Bank (2024); https://doi.org/10.57760/sciencedb.ecodb.00170
56. J. Kattge *et al.*, TRY plant trait database - enhanced coverage and open access. *Global Change Biology* **26**, 119-188 (2020).
57. M. L. Pruyn, B. L. Gartner, M. E. Harmon, Within-stem variation of respiration in (Douglas-fir) trees. *New Phytologist* **154**, 359-372 (2002).
58. R. Spicer, in *Vascular transport in plants,* M. Z. N Holbrook, Ed. (Elsevier Academic Press, Burlington, MA, USA, 2005), pp. 457–475.

59. R. Spicer, N. M. Holbrook, Parenchyma cell respiration and survival in secondary xylem: does metabolic activity decline with cell age? *Plant Cell and Environment* **30**, 934-943 (2007).
60. F. C. Meinzer, G. Goldstein, J. L. Andrade, Regulation of water flux through tropical forest canopy trees: Do universal rules apply? *Tree Physiology* **21**, 19-26 (2001).
61. J. Rodríguez-Calcerrada *et al.*, Stem CO_2 efflux in six co-occurring tree species: underlying factors and ecological implications. *Plant Cell and Environment* **38**, 1104-1115 (2015).
62. D. S. Falster *et al.*, BAAD: a Biomass And Allometry Database for woody plants. *Ecology* **96**, 1445-1445 (2015).
63. L. Plavcová, G. Hoch, H. Morris, S. Ghiasi, S. Jansen, The amount of parenchyma and living fibers affects storage of nonstructural carbohydrates in young stems and roots of temperate trees. *American Journal of Botany* **103**, 603-612 (2016).
64. M. Acosta, M. Pavelka, R. Pokorny, D. Janous, M. V. Marek, Seasonal variation in CO_2 efflux of stems and branches of Norway spruce trees. *Annals of Botany* **101**, 469-477 (2008).
65. O. K. Atkin, D. Bruhn, G. M. Tjoelker, in *Plant Respiration: From Cell to Ecosystem,* H. Lambers, M. Ribas-Carbo, Eds. (Springer Dordrecht, 2005), pp. 95-135.
66. M. A. Cavaleri, S. F. Oberbauer, M. G. Ryan, Wood CO_2 efflux in a primary tropical rain forest. *Global Change Biology* **12**, 2442-2458 (2006).
67. E. Darenova, P. Horácek, J. Krejza, R. Pokorny, M. Pavelka, Seasonally varying relationship between stem respiration, increment and carbon allocation of Norway spruce trees. *Tree Physiology* **40**, 943-955 (2020).
68. E. Darenova, J. Szatniewska, M. Acosta, M. Pavelka, Variability of stem CO_2 efflux response to temperature over the diel period. *Tree Physiology* **39**, 877-887 (2019).
69. M. G. Ryan, R. M. Hubbard, D. A. Clark, R. L. Sanford, Woody-Tissue Respiration for Simarouba-Amara and Minquartia-Guianensis, 2 Tropical Wet Forest Trees with Different Growth Habits. *Oecologia* **100**, 213-220 (1994).
70. S. T. Gower *et al.*, Carbon distribution and aboveground net primary production in aspen, jack pine, and black spruce stands in Saskatchewan and Manitoba, Canada. *Journal of Geophysical Research-Atmospheres* **102**, 29029-29041 (1997).
71. S. Tan, H. Wang, I. C. Prentice, K. Yang, Land-surface evapotranspiration derived from a first-principles primary production model. *Environmental Research Letters* **16**, 104047 (2021).
72. M. Cucchi *et al.*, WFDE5: bias-adjusted ERA5 reanalysis data for impact studies. *Earth Syst Sci Data* **12**, 2097-2120 (2020).
73. Z. C. Zhu *et al.*, Global Data Sets of Vegetation Leaf Area Index (LAI)3g and Fraction of Photosynthetically Active Radiation (FPAR)3g Derived from Global Inventory Modeling and Mapping Studies (GIMMS) Normalized Difference Vegetation Index (NDVI3g) for the Period 1981 to 2011. *Remote Sens-Basel* **5**, 927-948 (2013).
74. J. Chave *et al.*, Towards a worldwide wood economics spectrum. *Ecol Lett* **12**, 351-366 (2009).
75. African Wood Density Database, World Agroforestry Centre, Nairobi (2012); https://apps.worldagroforestry.org/treesnmarkets/wood/index.php#
76. G. Hoch, A. Richter, C. Körner, Non-structural carbon compounds in temperate forest trees. *Plant Cell and Environment* **26**, 1067-1081 (2003).
77. M. J. O'Brien, S. Leuzinger, C. D. Philipson, J. Tay, A. Hector, Drought survival of tropical tree seedlings enhanced by non-structural carbohydrate levels. *Nat Clim Change* **4**, 710-714 (2014).
78. J. S. Plavcová L, The role of xylem parenchyma in the storage and utilization of non-structural carbohydrates. *Functional and ecological xylem anatomy*, 209–234 (2015).

79. S. Salleo, M. A. Lo Gullo, P. Trifilò, A. Nardini, New evidence for a role of vessel-associated cells and phloem in the rapid xylem refilling of cavitated stems of Laurus nobilis L. *Plant Cell and Environment* **27**, 1065-1076 (2004).
80. A. R. Biggs, Occurrence and Location of Suberin in Wound Reaction Zones in Xylem of 17 Tree Species. *Phytopathology* **77**, 718-725 (1987).
81. G. Deflorio, C. Johnson, S. Fink, F. W. M. R. Schwarze, Decay development in living sapwood of coniferous and deciduous trees inoculated with six wood decay fungi. *Forest Ecology and Management* **255**, 2373-2383 (2008).
82. U. Schmitt, W. Liese, Response of Xylem Parenchyma by Suberization in Some Hardwoods after Mechanical Injury. *Trees-Structure and Function* **8**, 23-30 (1993).
83. A. L. Shigo, Compartmentalization — a Conceptual-Framework for Understanding How Trees Grow and Defend Themselves. *Annu Rev Phytopathol* **22**, 189-214 (1984).
84. R. Borchert, W. T. Pockman, Water storage capacitance and xylem tension in isolated branches of temperate and tropical trees. *Tree Physiology* **25**, 457-466 (2005).
85. N. M. Holbrook, in *Stems and trunks in plant form and function,* B. Gartner, Ed. (Academic Press, 1995), pp. 151–174.
86. M. Nawrot, W. Pazdrowski, M. Szymański, Dynamics of heart-wood formation and axial and radial distribution of sapwood and heartwood in stems of European larch (*Larix decidua Mill.*). *Journal of Forest Science*, 409–417 (2008).
87. I. Pinto, H. Pereira, A. Usenius, Heartwood and sapwood development within maritime pine (*Pinus pinaster* Ait.) stems. *Trees-Structure and Function* **18**, 284-294 (2004).
88. I. Burgert, A. Bernasconi, D. Eckstein, Evidence for the strength function of rays in living trees. *Holz Roh Werkst* **57**, 397-399 (1999).
89. I. Burgert, D. Eckstein, The tensile strength of isolated wood rays of beech (*Fagus sylvatica* L.) and its significance for the biomechanics of living trees. *Trees-Structure and Function* **15**, 168-170 (2001).
90. A. Reiterer, I. Burgert, G. Sinn, S. Tschegg, The radial reinforcement of the wood structure and its implication on mechanical and fracture mechanical properties - A comparison between two tree species. *J Mater Sci* **37**, 935-940 (2002).
91. M. A. Brodersen CR, Choat B, Matthews M, Shackel K, Dynamics of embolism repair in grapevine: in vivo visualisations using HRCT. *Plant Physiology*, 1088–1095 (2010).
92. G. G. Clearwater MJ, in *Vascular transport in plants,* M. Z. NM Holbrook, Ed. (Elsevier Academic Press, 2005), pp. 375–399.
93. S. Salleo, P. Trifilò, S. Esposito, A. Nardini, M. A. Lo Gullo, Starch-to-sugar conversion in wood parenchyma of field-growing plants: a component of the signal pathway for embolism repair? *Funct Plant Biol* **36**, 815-825 (2009).
94. S. Jansen *et al.*, Do quantitative vessel and pit characters account for ion-mediated changes in the hydraulic conductance of angiosperm xylem? *New Phytologist* **189**, 218-228 (2011).
95. A. Nardini, S. Salleo, S. Jansen, More than just a vulnerable pipeline: xylem physiology in the light of ion-mediated regulation of plant water transport. *Journal of Experimental Botany* **62**, 4701-4718 (2011).
96. M. Santiago, V. Pagay, A. D. Stroock, Impact of Electroviscosity on the Hydraulic Conductance of the Bordered Pit Membrane: A Theoretical Investigation. *Plant Physiology* **163**, 999-1011 (2013).
97. M. A. Zwieniecki, P. J. Melcher, N. M. Holbrook, Hydrogel control of xylem hydraulic resistance in plants. *Science* **291**, 1059-1062 (2001).
98. D. J. Hearn, T. Poulsen, R. Spicer, The Evolution of Growth Forms with Expanded Root and Shoot Parenchymatous Storage Is Correlated across the Eudicots. *Int J Plant Sci* **174**, 1049-1061 (2013).
99. S. Pfautsch, J. Renard, M. G. Tjoelker, A. Salih, Phloem as Capacitor: Radial Transfer of Water into Xylem of Tree Stems

Occurs via Symplastic Transport in Ray Parenchyma. *Plant Physiology* **167**, 963-+ (2015).
100. A. J. E. Vanbel, Xylem-Phloem Exchange Via the Rays - the Undervalued Route of Transport. *Journal of Experimental Botany* **41**, 631-644 (1990).
101. H. Yuan, Y. J. Dai, Z. Q. Xiao, D. Y. Ji, W. Shangguan, Reprocessing the MODIS Leaf Area Index products for land surface and climate modelling. *Remote Sens Environ* **115**, 1171-1187 (2011).
102. I. Harris, T. J. Osborn, P. Jones, D. Lister, Version 4 of the CRU TS monthly high-resolution gridded multivariate climate dataset. *Sci Data* **7**, 109 (2020).
103. S. P. Harrison *et al.*, Ecophysiological and bioclimatic foundations for a global plant functional classification. *J Veg Sci* **21**, 300-317 (2010).
104. I. C. Prentice *et al.*, A Global Biome Model Based on Plant Physiology and Dominance, Soil Properties and Climate. *J Biogeogr* **19**, 117-134 (1992).
105. I. C. Prentice, M. T. Sykes, W. Cramer, A Simulation-Model for the Transient Effects of Climate Change on Forest Landscapes. *Ecol Model* **65**, 51-70 (1993).
106. P. Kauppi, M. Posch, Sensitivity of Boreal Forests to Possible Climatic Warming. *Climatic Change* **7**, 45-54 (1985).
107. S. Tuhkanen, Climatic parameters and indices in plant geography. *Acta phytogeog* **16**, 1-105 (1980).
108. T. W. Davis *et al.*, Simple process-led algorithms for simulating habitats (SPLASH v.1.0): robust indices of radiation, evapotranspiration and plant-available moisture. *Geosci Model Dev* **10**, 689-708 (2017).
109. M. New, D. Lister, M. Hulme, I. Makin, A high-resolution data set of surface climate over global land areas. *Climate Res* **21**, 1-25 (2002).
110. O. Boucher *et al.*, IPSL IPSL-CM6A-LR model output prepared for CMIP6 ScenarioMIP ssp585, Earth System Grid Federation (2019);
https://doi.org/10.22033/ESGF/CMIP6.5271
111. O. Boucher *et al.*, IPSL IPSL-CM6A-LR model output prepared for CMIP6 ScenarioMIP ssp126, Earth System Grid Federation (2019);
https://doi.org/10.22033/ESGF/CMIP6.5262
112. G. Danabasoglu, NCAR CESM2 model output prepared for CMIP6 ScenarioMIP ssp126, Earth System Grid Federation (2019);
https://doi.org/10.22033/ESGF/CMIP6.7746
113. G. Danabasoglu, NCAR CESM2 model output prepared for CMIP6 ScenarioMIP ssp585, Earth System Grid Federation (2019);
https://doi.org/10.22033/ESGF/CMIP6.7768
114. S. Shim *et al.*, NIMS-KMA UKESM1.0-LL model output prepared for CMIP6 ScenarioMIP ssp585, Earth System Grid Federation (2021);
https://doi.org/10.22033/ESGF/CMIP6.8457
115. S. Shim *et al.*, NIMS-KMA UKESM1.0-LL model output prepared for CMIP6 ScenarioMIP ssp126, Earth System Grid Federation (2021);
https://doi.org/10.22033/ESGF/CMIP6.8433
116. T. Ziehn *et al.*, CSIRO ACCESS-ESM1.5 model output prepared for CMIP6 ScenarioMIP ssp126, Earth System Grid Federation (2019);
https://doi.org/10.22033/ESGF/CMIP6.4320
117. T. Ziehn *et al.*, CSIRO ACCESS-ESM1.5 model output prepared for CMIP6 ScenarioMIP ssp585, Earth System Grid

Federation (2019);
https://doi.org/10.22033/ESGF/CMIP6.4333
118. S. Sitch *et al.*, Trends and Drivers of Terrestrial Sources and Sinks of Carbon Dioxide: An Overview of the TRENDY Project. *Global Biogeochem Cy* **38**, e2024GB008102 (2024).
119. L. M. Silva *et al.*, The potential link between gas diffusion and embolism spread in angiosperm xylem: Evidence from flow-centrifuge experiments and modelling. *Plant Cell and Environment*, 4977-4991 (2024).
120. J. R. Schramski, A. I. Dell, J. M. Grady, R. M. Sibly, J. H. Brown, Metabolic theory predicts whole-ecosystem properties. *P Natl Acad Sci USA* **112**, 2617-2622 (2015).
121. P. G. Jarvis, in *Plant photosynthetic production. Manual of methods.,* W. N. Junk, Ed. (The Hague, 1971), pp. 566-631.
122. B. D. Stocker *et al.*, P-model v1.0: an optimality -based light use efficiency model for simulating ecosystem gross primary production. *Geosci Model Dev* **13**, 1545-1581 (2020).
123. J. Fox, S. Weisberg, An R Companion to Applied Regression, 3, (2019);
https://socialsciences.mcmaster.ca/jfox/Books/Companion/
124. J. R. Lockwood, D. F. McCaffrey, Correcting for Test Score Measurement Error in ANCOVA Models for Estimating Treatment Effects. *J Educ Behav Stat* **39**, 22-52 (2014).
125. J. R. Lockwood, D. F. McCaffrey, Simulation-Extrapolation with Latent Heteroskedastic Error Variance. *Psychometrika* **82**, 717-736 (2017).
126. S. Rabe-Hesketh, A. Pickles, A. Skrondal, Correcting for covariate measurement error in logistic regression using nonparametric maximum likelihood estimation. *Stat Model* **3**, 215-232 (2003).
127. M. M. Douglas Bates, Ben Bolker, Steve Walker, Fitting Linear Mixed-Effects Models Using lme4. Journal of Statistical Software. **67**, 1-48 (2019).
128. K. Bartoń, MuMIn: Multi-Model Inference, R package version (2024);
https://CRAN.R-project.org/package=MuMIn
129. P. Breheny, W. Burchett, Visualization of Regression Models Using visreg. *R J* **9**, 56-71 (2017).
130. H. Wickham *et al.*, ggplot2: Elegant Graphics for Data Analysis, (2009);
https://ggplot2.tidyverse.org
131. M. Campioli *et al.*, Evaluating the convergence between eddy-covariance and biometric methods for assessing carbon budgets of forests. *Nat Commun* **7**, 1-12 (2016).
132. M. Van Oijen, A. Schapendonk, M. Höglind, On the relative magnitudes of photosynthesis, respiration, growth and carbon storage in vegetation. *Annals of Botany* **105**, 793-797 (2010).

Acknowledgments: We thank Mark E. Olson and Christian Körner for comments on the preprint of this paper and acknowledge Allyson Eller for her contribution to data collection in Australia. We thank the editor and reviewers for valuable comments and suggestions.

Funding: This project is supported by

National Natural Science Foundation of China 42361144875 (HW)

National Key Research and Development Program of China 2023YFF1305500 (HW)

Hainan Institute of National Park Research Program KY-23ZK01 (HW)

Schmidt Sciences (HW, ICP, SPH, NGS, TK)

LLC, the Australian Research Council DP170103410 (ICP, IJW)

LLC, the Australian Research Council DP220102547 (IJW, HW)

LLC, the Australian Research Council CE200100015 (IJW)

the United States National Science Foundation DEB-2045968 (NGS)

the United States National Science Foundation DBI-2021898 (PBR)

the RUBISCO SFA, sponsored by the Regional and Global Model Analysis Program in the U.S. Department of Energy (DOE) Office of Science (T.F.K.)

DOE Early Career Research award (DE-SC0021023) (T.F.K.)

Author contributions:

Theory: H.Z., H.W., I.C.P., I.J.W., and S.P.H.

Data: H.Z., I.J.W., A.C.W., N.S., P.R., L.R., H.M., L.P. and S.J.

Investigation: H.Z., H.W., I.C.P., S.P.H., I.J.W., T.K. and N.B.N.

Visualization: H.Z.

Writing: original draft: H.Z., H.W., S.P.H.

Writing, review and editing: all.

Competing interests: Authors declare that they have no competing interests.

Data and materials availability: Data used in this study and original R code (version 4.0.2) used to analyze results have been deposited as a public archived databases (*55*) or in the Supplementary Materials.

Supplementary Materials

Materials and Methods

Figs. S1 to S11

Tables S1 to S15

References 56-132

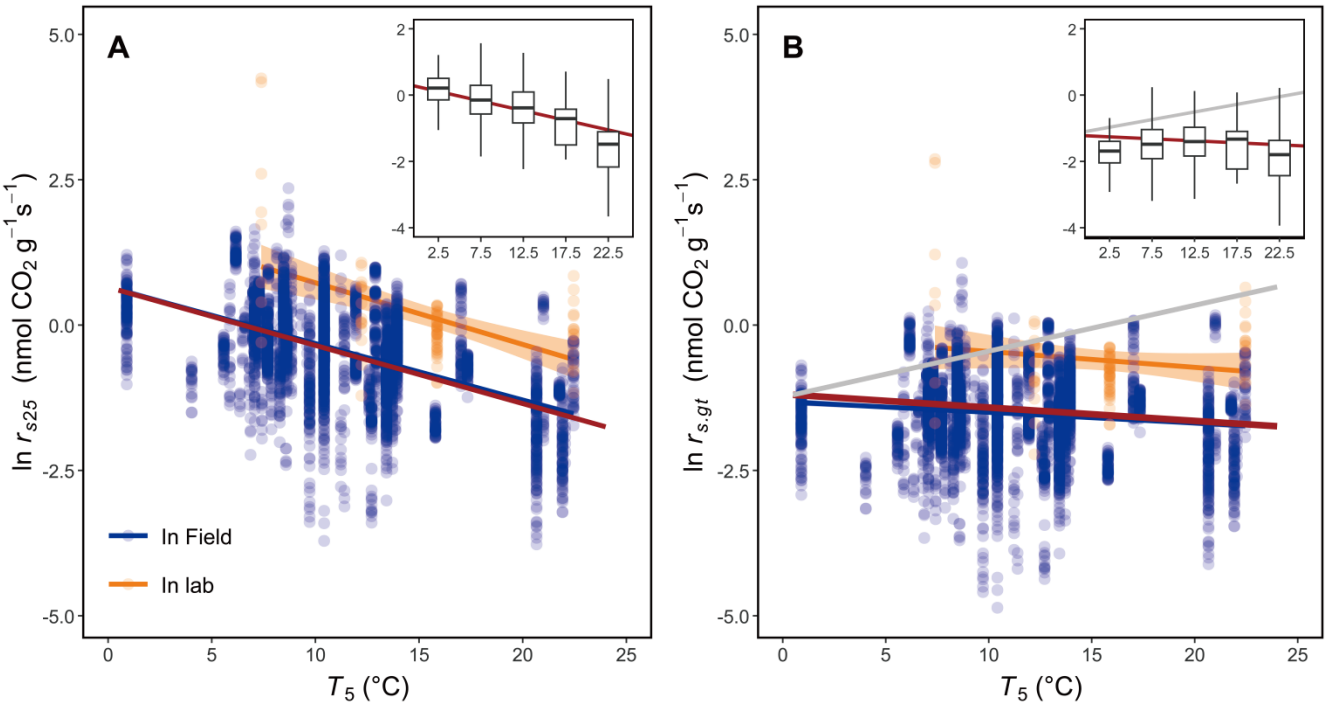

Fig. 1. Global trends of stem respiration at reference temperature (r_{s25}) and at growing temperature ($r_{s.gt}$) in relation to the mean value of the excess temperature above 5 °C (T_5). (A) Stem respiration was measured in the laboratory (orange circles) and in the field (blue circles). r_{s25} represents stem respiration standardized to the reference temperature of 25°C. Solid fitted lines are shown for the laboratory data (orange line), field data (blue line) separately (Statistical details are provided in Table 1). The shaded area represents the 95% confidence intervals. The solid red line is the theoretical prediction of thermal sensitivity, whose slope is −10.1% K^{-1}. The inset figure presents an overview of all the main figure data aggregated into temperature bins. Horizontal and vertical coordinates are the same as that in the main figure. **(B)** $r_{s.gt}$ represents stem respiration standardized to the mean growing temperature above 5 °C, using the same color coding as in (A). The solid red line is the theoretical prediction of thermal sensitivity of $r_{s.gt}$, whose slope is −2.3% K^{-1}. The instantaneous thermal response is also shown, based on a fixed-Q_{10} function (gray line). Noticeably, a value of 1 °C in T_5, for example, corresponds to a growing season mean temperature of 6 °C.

Quantity	Theoretical prediction	Measurements	Fitted coefficient	Confidence intervals		Intercept (mean ± SE)	R^2	p	df
				2.50%	97.50%				
r_{s25}	−0.101	In lab	−0.110	−0.143	−0.077	1.86 ± 0.57	0.27	<0.01	79
		In field	−0.101	−0.104	−0.099	0.70 ± 0.03	0.28	<0.001	4544
		All data	−0.098	−0.100	−0.095	0.67 ± 0.03	0.26	<0.001	4625
$r_{s.gt}$	−0.023	In lab	−0.028	−0.061	0.005	−0.17 ± 0.57	0.02	0.39	79
		In field	−0.019	−0.022	−0.017	−1.31 ± 0.03	0.01	<0.001	4544
		All data	−0.015	−0.018	−0.013	−1.33 ± 0.04	0.01	<0.001	4625

Table 1. Global trends of stem respiration in relation to temperature. Statistical output using the global dataset shown in Figure 1. r_{s25} represents stem respiration standardized to the reference temperature of 25°C; $r_{s.gt}$ represents stem respiration standardized to the mean growing temperature. Error in Variables regression analysis (EIV) was performed for field-based and lab-based data separately and also performed using all data. The table provides confidence intervals, R-squared values (R^2), p-values (p), and degrees of freedom (df) associated with each regression model.

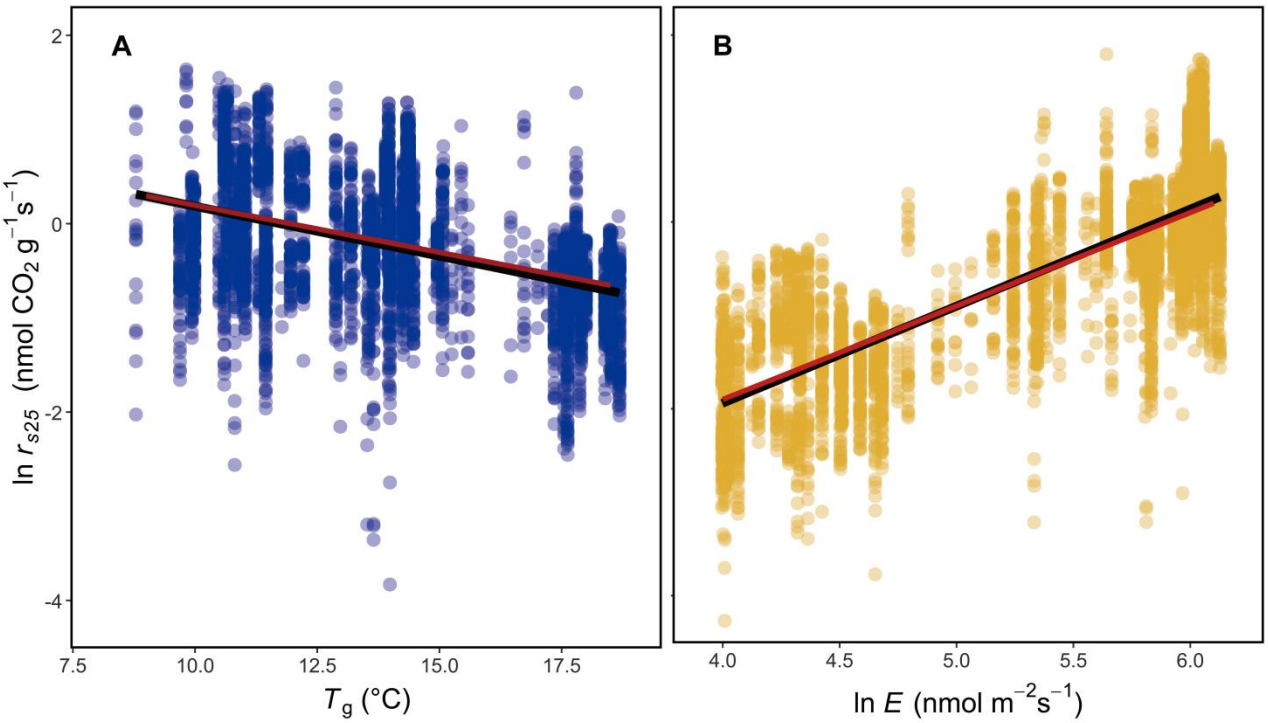

Fig. 2. Partial residual plots showing the relationship between stem respiration and temperature and transpiration when other factors are held constant. (A) Growth temperature (T_g) is an average of the six days before stem respiration was measured. r_{s25} is stem respiration, natural-log transformed, at the reference temperature of 25°C. **(B)** Transpiration (E) is an average of the thirteen days before measurement and was natural-log transformed. The solid black line is the relationship fitted via multiple regression ($\ln r_{s25} = (-0.106 \pm 0.005) \times T_g + (1.04 \pm 0.018) \times \ln E$, R^2=0.49, VIF=2.01, p<0.001). The red solid line is the theoretical prediction, with a coefficient of −10.1% K^{-1} and 100% (nmol H_2O m^{-2} s^{-1})$^{-1}$ for temperature and ln transpiration, respectively.

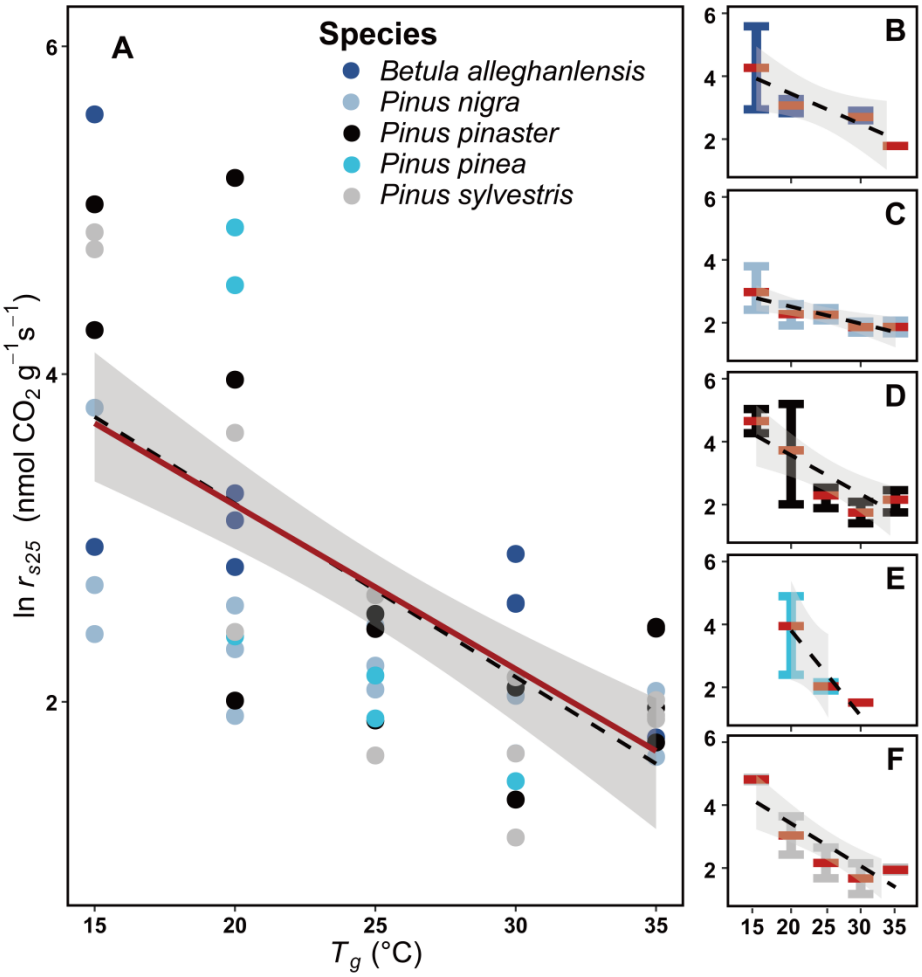

569

570 **Fig. 3. Relationship between stem respiration and growing temperature derived from a warming**
571 **experiment.** The warming experiment was conducted using five species: *Betula alleghaniensis*, *Pinus*
572 *nigra*, *Pinus pinaster*, *Pinus pinea* and *Pinus sylvestris*. **(A)** r_{s25} is stem respiration, natural-log
573 transformed, at the reference temperature of 25℃.Growth temperature (T_g) is the temperature at which
574 individual species were grown. Different colored points represent different species. The dashed line was
575 fitted ($\ln r_{s25} = (0.106 \pm 0.007) \times T_g$, R^2=0.44) using linear regression analysis on all the data. The red
576 solid line is the theoretical prediction, with a coefficient of −10.1%K^{-1}. **(B-F)** Box plots representing
577 different species, with colors consistent with those in (A). The short horizontal line represents the
578 maximum and minimum values, while the red short horizontal line represents the average value under
579 each T_g. The dashed line is the fitted line with shaded area representing the 95% confidence intervals.
580 Mathematical details are provided in table S8.

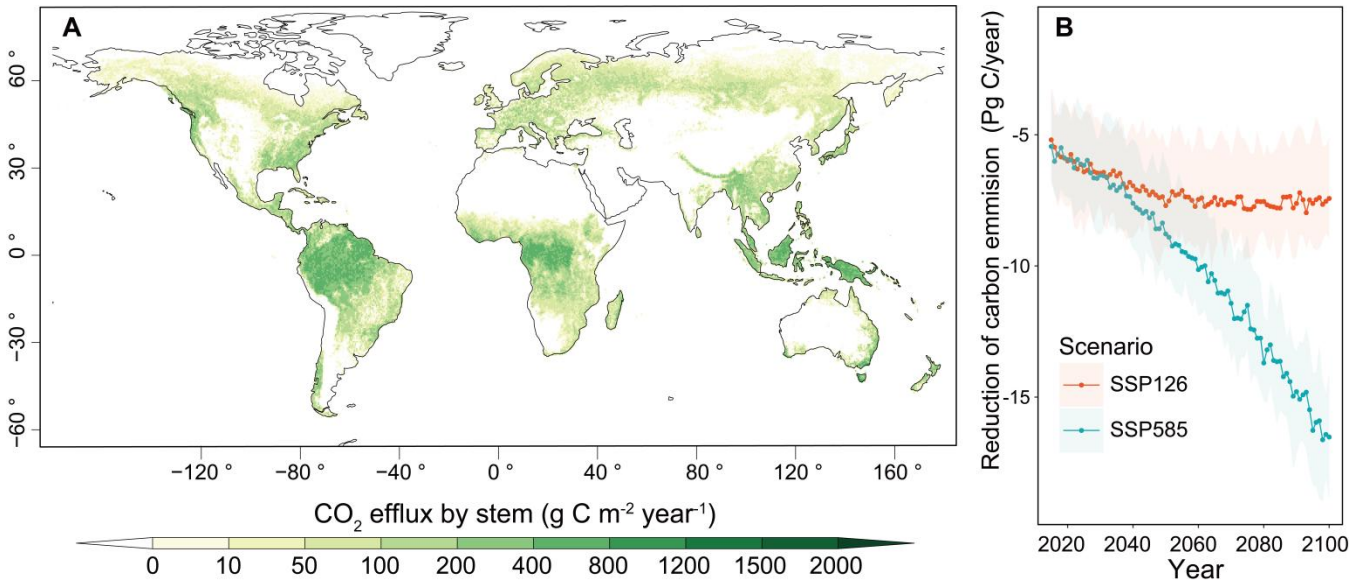

581

582 **Fig. 4. Predicted global stem respiration under present conditions and in response to future warming.**

583 **(A)** Stem respiration calculated at the global scale under recent CO_2 levels (see details in SI section 3.2).

584 **(B)** Simulated reduction in carbon emissions due to considering thermal acclimation of stem respiration

585 over the 21st century in two different scenarios (SSP126, SSP 585). The temperature was derived from an

586 ensemble of four future climate simulations (the land surface model is specified in brackets):

587 ACCESS−ESM1−5 (CABLE), CESM2 (CLM5), IPSL−CM6A−LR (ORCHIDEE) and UKESM1−0

588 (JULES). The solid dotted line is the mean ensemble value (orange: under SSP126, blue: under SSP585)

589 and the shaded area represents the range of the model ensemble.

590

Science
AAAS

Supplementary Materials for

Thermal acclimation of stem respiration implies a weaker carbon-climate feedback

Han Zhang[1], Han Wang[1*], Ian J. Wright[2,3,4], I. Colin Prentice[1,5], Sandy P. Harrison[1,6], Nicholas G. Smith[7], Andrea C. Westerband[2], Lucy Rowland[8], Lenka Plavcová[9], Hugh Morris[10], Peter B. Reich[11], Steven Jansen[12], Trevor Keenan[13,14], Ngoc Bao Nguyen[14]

*Corresponding author. Email: wang_han@tsinghua.edu.cn

The PDF file includes:

Materials and Methods
Figs. S1 to S11
Tables S1 to S15

Materials and Methods

1. Data and Pre-processing

1.1 Global Stem Respiration Dataset (GSRD)

1.1.1 Brief data description

The Global Stem Respiration Dataset (GSRD) includes: (a) data from existing datasets (TRY database, which includes the Functional Ecology of Trees (FET) dataset, ECOCRAFT dataset, Global Respiration Dataset, and Tropical Respiration Dataset) *(56)*, (b) data digitized from publications (journal articles and book chapters from 1966 to present), (c) data provided by colleagues listed in Acknowledgments, and (d) data provided by coauthors of this article. This compilation includes individual measurements of stem respiration rate (and other correlated traits) where species and site information were provided, and with sufficient information to be able to reasonably assign geographic coordinates, and thus climate data, for each sample. The records were screened according to the criteria described in table S1. Data records are presented in a table encompassing 9,887 rows and 33 columns. Each row represents an individual respiration rate datum, with each column reflecting a distinct variable including Reference, Site Location, Climate, Soil, Measurement, Plant Trait and Stem Respiration Rate. A detailed description of these columns are provided with the dataset. GSRD includes measurements from 109 sites worldwide on 320 species, and a total of 9886 observations.

To ensure all the data were processed in the same way, the records were further screened excluding observations without stem diameter information. After screening, we used a dataset that included measurements from 68 sites worldwide on 187 species, and a total of 4627 observations for global analysis and 4155 observations for seasonal analysis (table S2). The climate space represented in the dataset includes boreal, temperate, and tropical climate zones. The mean value of the excess temperature above 5°C, (T_5, see definitions in SI section 1.5) ranges from 0.9 to 22.5 °C. The range of estimated actual to potential evapotranspiration (α_p, AET/PET: characterizing aridity) is 0.06 to 0.62 (fig. S1).

Here, we quantified stem respiration as a process utilizing oxygen to oxidize glucose and other respiratory substrates for maintaining associated energy-requiring processes, including the maintenance of stem storage capacity, new xylem production, defense and resilience to disturbance, and the maintenance of stem water potential. We used stem respiration data measured as the rate of CO_2 emission from the stem surface of a woody plant. Although stem CO_2 efflux can be different from stem respiration as several post-respiratory processes (like CO_2 dissolution in xylem sap) affect the diffusion of locally-respired CO_2(*46-48*), stem CO_2 efflux (as compiled in the GSRD) is still an adequate proxy for this global meta-analysis. Most measurements were made in the field and some in the laboratory. 4546 observations of "In field" data from 63 sites were obtained either from the TRY Dataset or digitized from references (table S2). Stem respiration in the field was measured with a chamber attached to the surface of the trunk/branches and connected to an infrared gas analyzer (IRGA) to record the variation of CO_2 concentration. Stem diameters, when reported, ranged from 10.03 to 148 cm, with a mean and standard deviation of 25.9 ± 12.0 cm. Our data set also includes 81 laboratory measurements on species from four sites (ca. 1.8% of the data set) provided by TRY Dataset and co-authors (table S2). These measurements were made using tissues excised from wood cores or branches removed from the field and transported back to the laboratory for mass-based sapwood respiration measurements, also conducted using an infrared gas analyzer. Although the total sample size of the laboratory measurement dataset is small, it has the advantages of unified measurement units, measurement sites, and small data errors. The field dataset is relatively complex, with inconsistent measurement locations and units, but has the advantages of a larger data volume, greater species coverage, and a wider distribution of sample sites across climate gradients.

1.1.2 Pre-processing by converting area-based to mass-based stem respiration

Only the living cells within the stem are responsible for CO_2 emission, of which sapwood is the most important component. The fraction of dead (non-respiring) heartwood should be excluded in calculation, particularly in large-sized trees, as trees uniquely maintain several active rings for water transport(*57-59*), and the fraction of (non-respiring) heartwood increases with tree size. Here, we included an allometric equation to estimate sapwood area based on stem diameter (*43, 46, 60, 61*).

$$A_{sap} = a_0 \times A_{stem}^{b_0} = a_0 \times \left(\frac{\pi}{4} \times D^2\right)^{b_0} = \frac{a_0 \times \pi^{b_0}}{4^{b_0}} \times D^{2 \times b_0} \quad (1)$$

where A_{sap} is the tree-level sapwood cross-sectional area. D is tree trunk diameter at breast height. a_0 and b_0 are allometric parameters fitted using measurements taken at breast height contained from a biomass and allometry database (BAAD) and other literature sources (*43, 60, 62*). For data from tropical, temperate and northern hemisphere trees, the relationship between sapwood area and diameter indicates relatively conservative allometric parameters.

The volume and surface area of a tree stem can be calculated as follows,

$$V_{stem} = \frac{1}{n} \times A_{stem} \times h \quad (2)$$

$$S_{stem} = 2 \times \pi \times \int_0^h f(x) \times dx = 2 \times \pi \times \int_0^h \frac{r_{stem}}{h^{\frac{n-1}{2}}} \times x^{\frac{n-1}{2}} \times dx = \pi \times D \times \frac{2}{n+1} \times h \quad (3)$$

where V_{stem} is the volume of entire tree. n describes the shape of the tree stem (e.g., cylinder, n=1; paraboloid, n=2; cone, n=3; neiloid, n=4) and h is the height of the tree stem. S_{stem} is the surface area of entire tree. r_{stem} and D are radius and diameter of basal stem.

We could further express sapwood volume as a function of A_{sap}, the factor n , h and the allometric exponent b_0 as follows,

$$V_{sap} = \frac{1}{(n-1) \times b_0 + 1} \times A_{sap} \times h \quad (4)$$

We then standardized measurements from area-based to mass-based stem respiration rates when necessary, by combining Eqs. 1-3, according to Eq. 4.

$$r_{s_mass} = \frac{r_{s_area} \times S_{stem}}{m_{sap}} = \frac{r_{s_area} \times \frac{2}{n+1} \times \pi \times D \times h}{\rho_s \times V_{sap}} = \frac{r_{s_area} \times D^{1-2 \times b_0}}{\rho_s} \times \frac{2 \times 4^{b_0} \times \left[(n-1) \times b_0 + 1\right] \times \pi^{1-b_0}}{a_0 \times (n+1)} \quad (5)$$

where r_{s_mass} and r_{s_area} are mass-based and surface-area-based stem respiration rates respectively (nmol CO_2 g^{-1} s^{-1} and μmol CO_2 m^{-2} s^{-1}). S_{stem} is the tree-level stem surface area. m_{sap} is mass of sapwood. h is tree height. V_{sap} is tree-level sapwood volume. ρ_s is wood density (g m^{-3}); D is the diameter of the stem at the measuring point, i.e. breast height (~1.3m); n is assumed as a mean value of 2.5, reflecting the mean value of the most common shapes of a paraboloid (n=2) and a cone (n=3) (*43*). The allometric parameters a_0 and b_0 here refer to 0.365 and 0.877 respectively, using measurements contained in the BAAD (*43*).

We also used existing parenchyma tissue fraction data to estimate the mass of respiring stem as a supplement, using a global data set compiled by Morris et al. (*36*), for there was a limited amount of data on the fraction of living cells within the stem, for individuals or even species. Other living cells, including living fibers, may contribute to stem respiration. However, parenchyma is the largest contributor to respiration for most species (*63*). We therefore use parenchyma tissue fraction (RAP, including ray

parenchyma and axial parenchyma tissue fractions, SI section 1.4) as a proxy for the relative mass of respiring stem tissue in sapwood and calculate parenchyma mass-based stem respiration by dividing Eq. 5 with RAP. Considering the differences in RAP between angiosperm and gymnosperms separately, we consider constants of 7.6% and 24.6% for them, respectively. Whether this parenchyma tissue fraction is considered, or not, has very little effect on the thermal sensitivity of mass-based stem respiration. For parenchyma mass-based stem respiration, both gymnosperms and angiosperms show similar thermal acclimation at a rate that is consistent with our theoretical predictions, even though the respiration rate in gymnosperms is systematically higher than that in angiosperms (fig. S9 and table S14) due to the anatomical differences.

1.1.3 Pre-processing by temperature standardization

The measurement temperatures in the GSRD ranged from 0.5 to 41.5 ℃, with a mean and standard deviation of 17.91±7.1℃. The respiration rate at a standard temperature (such as 25℃) is generally used to compare across different environments, and can be obtained using a fixed-Q_{10} exponential equation (*8*), describing the instantaneous response derived from enzyme kinetics alone.

$$r_{Tref} = r \times Q_{10}^{\frac{T_{ref}-T}{10}} \quad (6)$$

where r_{Tref} is the respiration rate at the reference temperature (mol CO_2 g^{-1} s^{-1}), and r is the respiration rate at the measurement temperature (mol CO_2 g^{-1} s^{-1}). T_{ref} and T (here we used 25℃) are the reference temperature and measurement temperature, respectively. Q_{10} is the thermal sensitivity of respiration, which is a fixed value that represents the increase in respiration rate for a 10℃ increase in temperature. We used a fixed Q_{10} of 2.2 (*64, 65*). The kinetic thermal sensitivity without considering acclimation can be calculated by taking the logarithm of Eq. 6 (grey line in Fig. 1B).

$$\ln r_{Tref} = -0.1 \times \ln Q_{10} \times (T - 25) + \ln r = -0.079 \times (T - 25) + \ln r \quad (7)$$

1.1.4 Uncertainty in stem respiration observations

The uncertainties in stem respiration observations include assumptions about mean stem diameter values. For those samples without individual measured diameters, we used the mean stem diameter reported in the original literature. We further clarified that the relationship between diameter and T_5 in global-scale analyses had little effect on the results of stem respiration thermal sensitivity. Stem diameter has a weak relationship with T_5 (R^2=0.016) when using the diameters of samples for which we had measurements of stem respiration (table S12), rather than stand-level mean stem diameter. Furthermore, multiple regression analysis of 'in field' measurements on r_{s25} with trunk diameter and T_5 showed that diameter further explained 4% variations in r_{s25} (table S13), in addition to the 28% variations explained by T_5 only (Table 1). Additionally, the parameters a_0 and b_0 introduced during the allometric process also contribute to uncertainties, which were fitted to the measurements contained in the BAAD, estimated by generalized non-linear least square regression. We used the square root of the variance of the residuals from the fitted allometric models in Thurner et al. to calculate standard error of a_0 and b_0 (0.051 and 0.029) (*43, 62*). As for the uncertainty introduced by the Q_{10}, we carried out subsequent tests in which the Q_{10} was changed from 1.6 to 2.8 (*57, 64-69*) showing that using different Q_{10} values had no substantial impact on the theoretical prediction effect of thermal sensitivity (table S11).

1.2 Temporal data

1.2.1 Stem respiration data

We also analyzed information from time series records on stem respiration. Lavigne and Ryan measured stem respiration during the 1994 growing season at eight sites with contrasting climates (*20, 69, 70*). We obtained data from one site near the northern boundary of the boreal region, close to Thompson, Manitoba (55.90°N, 98.75°W) from the TRY dataset, where measurements were made between May to September 1994. There were 4155 observations for seasonal analysis, including the species black spruce, aspen and jack pine (table S2).

1.2.2 Transpiration data

Transpiration data used in our seasonal analysis was calculated using the Penman-Monteith equation driven by daily radiation, temperature, vapor pressure deficit, atmospheric pressure and leaf area index. Stomatal conductance in the Penman-Monteith equation was estimated based on GPP and the ratio of leaf-internal to ambient CO_2 partial pressure, both of which were calculated by the EEO-based P model (*41, 71*). The P model assumes an optimal stomatal behaviour allowing plants to minimize the total costs of maintaining the capacities for carboxylation and transpiration (*33*). This results in a predicted canopy-level stomatal conductance that is a function of temperature, vapor pressure deficit, atmospheric pressure, radiation and leaf area index. Embolism risk is not considered explicitly, assuming that this is already accounted for through stomatal control. The potential influences of those driven variables on stem respiration are therefore implicitly considered via transpiration. Other potential environmental factors, such as soil moisture, were not considered due to data limitations.

Daily shortwave downward radiation, atmospheric pressure in the horizontal plane, atmospheric water vapor pressure deficit, and near-surface temperature for the site (55.90º N, 98.75º W) were calculated from the extracted hourly data in WFDE5 (Watch Forcing Data methodology applied to ERA5) (*72*). The fraction of absorbed photosynthetically active radiation (fAPAR) was extracted from the fortnight data in GIMMS-3G (Global Inventory Monitoring and Modeling System, FPAR3g) at resolution of 1/12º (*73*) and linearly interpolated to a daily scale. Averaged transpiration at different time scales ranging from 1 to 21 days was calculated to explore at what time scale stem respiration acclimated to the prior transpiration status. Averaged temperature at different time scales were calculated with same algorithm based on data extracted from WFDE5.

1.3 Warming experiment data

A warming experiment was conducted by Smith et al. (*12*). They examined the thermal acclimation of stem respiration in individuals of five different woody species acclimated to five temperatures: 15, 20, 25, 30, 35 ℃. They also conducted instantaneous tissue temperature response curves (at 14, 23, 32, 41, ~50 ℃) on each individual following a 7-day acclimation period. We selected data for woody saplings only, with a single specimen acclimated to each temperature. We used measured instantaneous thermal response to calculate stem respiration at 25℃ and growing temperature by the following equation,

$$R_T = \exp\left(c_1 + c_2 \times T + c_3 \times T^2\right) \quad (8)$$

where R_T (μmol g^{-1} s^{-1}) is the stem respiration rate at the stem temperature T (℃), c_1 corresponds to the exponential rate of R_T at 0℃, c_2 and c_3 are parameters describing the change with increasing temperature.

1.4 Auxiliary trait-related data

We used the World Flora Online (https://www.worldfloraonline.org/), the Flora of China

(http://www.iplant.cn/foc) and the Plant List (http://www.theplantlist.org/) for species identity. The authority were also added to avoid any synonyms and taxonomic problems/misidentification, or recent/future taxonomic changes, based on the Plant List. We categorized species into plant functional types (PFTs), according to permanence of above-ground living biomass, leaf longevity (evergreen vs. deciduous) and leaf structure (broad-leaved vs. needle-leaved). This resulted in four PFTs: evergreen broad-leaved, deciduous broad-leaved, deciduous needle-leaved, and evergreen needle-leaved. We assigned each species to a PFT using information from the World Flora Online, the Flora of China and the Plant List.

We included information on wood density for each species, which represents the dry mass of wood per stem fresh volume. Wood density is an important trait for estimating stored biomass and carbon content per unit volume of tree stem (*74*). Wood density data were obtained from the TRY database and the African Wood Density Database (https://apps.worldagroforestry.org/treesnmarkets/wood/index.php) (*56, 75*). The standard deviation of wood density within each species varied from near 0 to 17.6%, meanwhile 91.3% of the species we used had a standard deviation of less than 10%. This suggests wood density is conservative within species. We thus used the mean value of each species in our analyses. Where species-specific values were not available we used the mean value for the genus.

Morris et al. assembled a dataset of wood parenchyma fraction (RAP) for 1439 species (*36*), in which there was a relationship between parenchyma tissue fraction and site temperature. Applying this relationship in the process of converting the stem respiration to a mass-based value had little effect on the value of fitting sensitivity (table S14). As a simplification, given the 3-fold difference in RAP between angiosperms (24.6%) and conifers (7.6 %), we include the two constants as an expression of RAP.

Box1. Functions related to xylem parenchyma (including ray and axial parenchyma) in wood.

Storage and transport of nonstructural carbohydrates (NSCs) (*76-79*).
Defence against pathogens (*80-83*).
Water storage and xylem hydraulic capacitance (*84, 85*).
Storage of mineral inclusions.
Transition of functional sapwood to heartwood (*58, 86, 87*).
Mechanical contributions, particularly by ray parenchyma (*88-90*).
Embolism repair (*91-93*).
Ion-mediated enhancement of xylem hydraulic conductance via the release of inorganic species such as K^+ and Ca^{2+} into the transpiration stream (*94-97*).
Providing means for interactions between phloem and xylem (*59, 98-100*).

Biomass data used to simulate global stem respiration were from the Global Biomass Data Product (GBDP, available at https://doi.org/10.1594/PANGAEA.894711) (*42*). This forest map has a pixel size of 1 ha and is based on satellite remote sensing observations from the year 2010 (±1year). We used the estimates of above ground biomass (AGB, unit: Mg/ha), which is defined as the dry weight of stem, bark, branches and twigs from living plants (i.e. excluding dead stumps or roots). The datasets included estimates of the per-pixel uncertainty expressed as standard error in Mg/ha. The forest land cover information is extracted from the Moderate Resolution Imaging Spectroradiometer (MODIS) land cover product (MCD12C1) in 2010, including pixels of Evergreen needleleaf forests, evergreen broadleaf forests, deciduous needleleaf forests, deciduous broadleaf forests and mixed forests downloaded from LDAAC

database (https://lpdaac.usgs.gov/) (*101*).

1.5 Environmental data

Site locations (latitude, longitude) were taken from source publications or estimated from information given therein (WGS84 datum adopted as standard). Where published coordinates did not fall in the correct country or fell in water rather than land (based on the climate raster layers), new coordinates were estimated (from Google Earth) based on site descriptions or simply moved to the nearest terrestrial suitable grid-cell on the Worldclim v1.3 raster layer, matching source and model elevation as closely as possible.

Temperature data for the period 1901 to 2018 were extracted from CRU TS (Climatic Research Unit gridded Time Series) version 4.02, which has a spatial resolution of 0.5º latitude by 0.5º longitude over all continents except Antarctica, and a daily temporal resolution (*102*). All plants require a period with temperatures sufficient for growth, as represented by measures of accumulated growing-season warmth. Here we use the mean value of the excess temperature above 5℃ (T_5), calculated by the following equation (*103-105*),

$$T_5 = \frac{\sum_{1}^{N}(T_{air} - 5)}{N} \quad (9)$$

where T_{air} is the daily air temperature (when $T_{air} \geq 5$℃). N is the length of the growing season defined as the length of the interval with T_{air} more than 5℃, which is the approximate minimum temperature for tree growth (*106, 107*). Noticeably, T_5 is defined as the mean value of excess temperature above 5 ℃. Therefore, a value of 1℃ in T_5, for example, corresponds to the mean temperature of the growing season as 6℃, rather than 1℃. Although the CRU CL v2.0 dataset has a higher spatial resolution, its monthly temporal resolution would cause larger uncertainty in calculating T_5. We also calculated α_p, the ratio of actual evapotranspiration to potential evapotranspiration using the SPLASHv1.0 model (*108*). The inputs to this model are elevation, monthly temperature, monthly sunshine hours and monthly precipitation, sourced from CRU CL v2.0 (*109*). Vapor pressure deficit was calculated using relative humidity, elevation and temperature from CRU CL v2.0 (*109*).

1.6 Climate Model Outputs+

We simulated stem respiration using future climate projections from CMIP6 (Coupled Model Inter-comparison Project Phase 6), following two of the Shared Socioeconomic Pathways (SPP126 and SSP585) during the period of 2015−2100. SSP126 represents a future scenario of anthropogenic policies in which there is strong action to reduce greenhouse gas emissions, which therefore leads to a moderate warming. SSP585 represents a business-as-usual scenario with high greenhouse gas emissions, leading to a more dramatic warming. We used four Earth System Models that have the necessary outputs for these analyses: ACCESS−ESM1−5, CESM2, IPSL−CM6A−LR and UKESM1−0, whose Land Surface Models are CABLE2.2.3, CLM5, ORCHIDEEV2.0 and JULES−ES−1.0 (*110-117*). We extracted near-surface temperature outputs to calculate T_5. We also used estimates from nine TRENDY models (version 9, 2021, scenario 2) (*118*) for comparing the global simulation result, including CABLE-POP, CLASSIC, CLM5.0, ISAM, LPJ-GUESS, LPX-Bern, ORCHIDEE, ORCHIDEE-CNP and SDGVM.

2. Theoretical derivation

2.1 Principles of theory predicting thermal sensitivity

Under the assumption that a primary function of sapwood is maintaining the hydraulic continuum as determined by the canopy water demand, we assumed that the cost of doing so – whole-plant stem respiration – is proportional to transpiration from the canopy on a timescale of days to weeks,

$$R_s = a \times E_{sap} = a \times E_{canopy} \quad (10)$$

where R_s (μmol CO_2 s^{-1}) is the whole-plant stem respiration, E_{sap} (μmol H_2O s^{-1}) is the sap flow through the stem tissue, E_{canopy} is the canopy-scale transpiration, and a is a cost factor representing the respiration rate required to support a unit transpiration rate. To maintain the hydraulic continuum, E_{sap} equals E_{canopy}; henceforth we simply use the symbol, E. Here transpiration refers to actual transpiration influenced by various variables including *VPD* and stomatal behavior.

$$R_s = a \times E \quad (11)$$

R_s is also a product of the respiration rate per unit mass (r_s, nmol CO_2 g^{-1} s^{-1}) and the total sapwood mass (M_s, g C). The mass-based stem respiration rate is an enzyme-mediated process, which can be expressed by the fixed-Q_{10} equation as *f(T)*, describing the kinetic thermal response (Eq. 6). In order to compare species and individuals, we converted the measurements to a reference temperature of 25°C, so that r_{s25} is mass-based stem respiration rate at the reference temperature of 25°C.

$$R_s = r_{s25} \times f\left(T\right) \times M_s \quad (12)$$

$$f\left(T\right) = Q_{10}^{\frac{T-T_{ref}}{10}} \quad (13)$$

The cost factor that describes the expense of transporting water up to the canopy is also theoretically influenced by temperature as the viscosity of water decreases with increasing temperature, resulting in lower costs to support a specific rate of hydraulic supply and, consequently, reduced transpiration rate. We thus expressed a_{25} as the respiration cost of transpiration at 25°C. Variation in the viscosity of water in relation to temperature followed Eq. 15. Eq. 15 itself was derived from the Vogel equation at a standard temperature of 25°C (*33, 39*).

$$a \times E = a_{25} \times \eta\left(T\right) \times E \quad (14)$$

$$\eta\left(T\right) = e^{0.0226 \times \left(25-T\right)} \quad (15)$$

Note that we omit the effect of temperature on the surface tension of water, and hence on the potential risk of embolism, because this is small (*ca*. 1.5% increase in P_{50} for water temperature increasing from 5 to 15 °C, and a 1.7% increase in P_{50} for water temperature increasing from 20 to 30 °C) (*119*).

Combining Eqs. 10-15 and taking logarithms on both sides, Eq. 11 can then be re-written as Eq. 16, from which we derive the linear equation, Eq. 17.

$$r_{s25} \times f\left(T\right) \times M_s = a_{25} \times \eta\left(T\right) \times E \quad (16)$$

$$\ln r_{s25} + 0.1 \times \ln Q_{10} \times \left(T-25\right) + \ln M_s = \ln a_{25} + 0.0226 \times \left(25-T\right) + \ln E \quad (17)$$

By re-arranging this equation, we obtain the general formula describing r_{s25}.

$$\ln r_{s25} = -0.1 \times \left(T-25\right) + \ln a_{25} + \ln E - \ln M_s \quad (18)$$

At a weekly to seasonal time scale, we assumed that r_s is proportional to both E and the cost factor at a time scale when M_s almost remains unchanged.

$$\ln r_{s25} = -0.1 \times \left(T-25\right) + \ln a_{25} + \ln E + C_1 \quad (19)$$

where C_1 is a constant.

When variations in M_s are too large to be ignored, as happens when considering spatial patterns, metabolic theory suggests that this variation would be canceled out due to variation in E over the same time scale (*120*). Consequently, we expect r_s to be exclusively proportional to the cost factor, whereas its thermal acclimation behavior remains at the short time scale.

$$\ln r_{s25} = -0.1 \times (T - 25) + \ln a_{25} + C_2 \tag{20}$$

where C_2 is a constant. This equation generates a prediction that r_{s25} declines with growth temperature by 10.1% K^{-1}.

In addition to the thermal sensitivity of r_{s25}, we also examined variation in respiration at growth temperature, $r_{s.gt.}$ We can express $r_{s.gt}$ as a function of temperature, through the effect of variation in water viscosity. In this case, r_s at the growth temperature acclimates ($r_{s.gt}$, nmol CO_2 g^{-1} s^{-1}) to track the thermal response of the cost factor as determined by water viscosity. This prediction means $r_{s.gt}$ declines with temperature by 2.3% K^{-1}.

$$r_{s.gt} \times M_s = a_{25} \times \eta(T) \times E \tag{21}$$

$$\ln r_{s.gt} = -0.023 \times (T - 25) + \ln a_{25} + \ln E \tag{22}$$

2.2 Theoretical prediction of sensitivity to vapor pressure deficit

Although it is difficult to disentangle the effects of temperature and vapor pressure deficit (*VPD*), we implement E as a function of stomatal conductance (g_s) and *VPD*, to express water demand at the canopy scale.

$$E = 1.6 \times g_s \times \frac{VPD}{P_{atm}} \tag{23}$$

where *VPD* is vapor pressure deficit (Pa), P_{atm} is the atmospheric pressure (Pa) and g_s is stomatal conductance to CO_2 (mol m^{-2} s^{-1}), which is tightly regulated and depends on environmental conditions. The value 1.6 in the equation represents the H_2O/CO_2 conductance ratio (*121*). By balancing the costs associated with maintaining the transpiration stream and the cost of a given carboxylation capacity, the P-model predicts the optimal ratio of leaf-internal to ambient CO_2 concentration c_i:c_a, and then the *GPP* or g_s values as follows (*33, 39, 122*).

$$g_s = \frac{GPP}{c_{mol_mass} \times (c_a - c_i)} \tag{24}$$

$$GPP = \varphi_0 \times I_{abs} \times m \times \sqrt{\left[1 - \left(\frac{c^*}{m}\right)^{\frac{2}{3}}\right]} \tag{25}$$

where

$$m = (c_a - \Gamma^*) \Big/ \left\{ c_a + 2 \times \Gamma^* + 3 \times \Gamma^* \times \sqrt{1.6 \times \eta^* \times D_0 \times \beta^{-1} \times (K + \Gamma^*)^{-1}} \right\} \tag{26}$$

$$c_i = \frac{\xi \times c_a + \Gamma^* \times \sqrt{VPD}}{\xi + \sqrt{VPD}} \tag{27}$$

where

$$\xi = \sqrt{\frac{\beta \times \left(K + \Gamma^*\right)}{1.6 \times \eta^*}} \quad (28)$$

where *GPP* is gross primary production (g C m^{-2} $month^{-1}$), c_{mol_mass} is the molecular mass of carbon (g), c_i and c_a are ambient and internal CO_2 concentrations, φ_0 is the intrinsic quantum yield (1.02 g C mol^{-1}), I_{abs} is the absorbed photosynthetic photon flux density (*PPFD* mol m^{-2} s^{-1}), Γ^* is the photorespiratory compensation point (Pa), K is the effective Michaelis–Menten coefficient of Rubisco (Pa), η^* is the viscosity of water relative to its value at 25℃, β^* is the ratio of carboxylation to transpiration cost factors at 25 ℃, ≈146 (*33, 122*), and c^* is a constant proportional to the unit carbon cost for the maintenance of electron transport capacity, ≈0.41. The theory underlying optimal *GPP* was described in Wang et al.(*33*) and Eqs. 23-28 show the relationship with *VPD*.

By taking partial derivatives of *VPD* in Eq. 16, we obtain the theoretical formula for the sensitivity of r_{s25} to *VPD*.

$$\frac{\partial \ln r_{s25}}{\partial VPD} = \frac{\partial \ln E}{\partial VPD} = \frac{\partial\left(1.6 \times g_s \times \frac{VPD}{P_{atm}}\right)}{\partial VPD} \quad (29)$$

Combining Eqs. 23-29, in order to see the complex effect of *VPD* on r_{s25}, we carried out sensitivity analysis of ln r_{s25} to ln *VPD*, by setting the temperature as 25℃, atmospheric pressure as 101325 Pa, *fAPAR* as 1, *PPFD* as 300 mol m^{-2} $month^{-1}$ and *VPD* varying from 50 to 1000 Pa. All else equal, ln r_{s25} has a nearly linear relationship with ln *VPD*, with a sensitivity ≈0.54 Pa^{-1} (fig. S10).

3. Methods

3.1 Statistical analysis

The stem respiration rate data, site-transpiration data and vapor pressure deficit data were natural log-transformed for analysis. To compare between field and lab data, we employed Analysis of Variance (ANOVA) to assess the variation between different measurement groups (table S4). We determined the timescale of seasonal acclimation using R-squared, Root Mean Square Deviation (RMSE) and Variance Inflation Factors (VIF). We chose a 6-day time window for temperature and a 13-day time window for transpiration because this combination had higher R-squared and lower RMSE with relatively low collinearity (VIF), together indicating the best fitting model (fig. S5 and table S7). Calculations were performed using the R package *car version 3.1-2 (123).*

Errors-in-variables (EIV) regression is a standard method for consistent estimation in linear models with noisy covariates (*124-126*). We used the R package *eivtools* (Lookwood) for analysis of the relationship between r_{s25} or $r_{s.gt}$ and T_5, at the global scale (Fig. 1, Table 1, fig. S9 and table S14). We calculated the reliability (which is 100% minus the ratio of the standard deviation to the mean) including the time mismatch estimated by differences over 30 years, and the spatial mismatch calculated by comparison with the CRU CLv2.0 data. After applying error transfer equations, the reliability of global T_5 was estimated as 0.96. We also used Linear Mixed Models (LMM) as a supplement, considering different group or measurements as random effects (table S3). These calculations were performed using the R package *lme4 version 1.1-35.5 (127)* and *MuMIn version 1.48.4 (128).* EIV regression analysis was also carried out on data without temperature standardization, all measurements on *Pinus,* diameter related analysis and (figs. S3-4 and table S). We conducted linear regression analysis on site-mean data, considering different measuring methods as an influencing factor (fig. S2 and table S5). At seasonal scale, we carried out multiple regression analysis between natural log-transformed stem respiration value and temperature and transpiration using base R (Figure 2, figs. S5-6 and table S7). For the warming experiment,

we conducted regression analyses separately for individual species and for the entire dataset, also using base R (Figure 3, fig. S8 and table S8). All plotting was done using the R packages *visreg* and *ggplot2 (129, 130)*.

3.2 Modelling and simulation

3.2.1 A simple model of stem respiration at ecosystem scale

To obtain an overall estimate of stem respiration, we up-scaled individual-scale mass-based r_s to the ecosystem scale. We developed a simple model to simulate global stem respiration taking thermal acclimation into account.

$$F_s = \sum_{i=1}^{n} R_s \times Area \times Time_{growth} = \sum_{i=1}^{n} r_{s25_sap} \times f(T) \times m_{sap} \times Area \times Time_{growth} \quad (30)$$

where F_s is the annual carbon dioxide emission by stem respiration globally (unit: Pg CO_2). R_s is land-area-based stem respiration (nmol CO_2 m^{-2} s^{-1}), and r_{s25_sap} is sapwood mass-based stem respiration at a reference temperature of 25°C (nmol CO_2 g^{-1} s^{-1}), where we introduced thermal acclimation. *f(T)* follows a fixed-Q_{10} equation, representing the instantaneous thermal response, where T is T_5. m_{sap} (above-ground sapwood biomass (g ha^{-1}), and *Area* (grid cell area, m^2) were used to calculate the respiring stem mass of each pixel. $Time_{growth}$ (growing season) was defined as the period during the year when the mean temperature is above 5°C.

We obtained the value of r_{s25_sap} via calibration with data from the Global Stem Respiration Database (GSRD), where the measurement temperature was 25±1°C (table S10). We first convert living cell mass-based stem respiration to sapwood mass-based stem respiration. By fixing the slope to 0.1 (which is the theoretical thermal sensitivity of stem respiration rate at 25°C, Eq. 18), we modeled ln r_{s25_sap} as a linear function of T_5. Stem respiration at the reference temperature can be predicted by T_5, with the estimated value of C being 0.53 from this calibration. The standard error of the r_{s25_sap} equals that of the intercept, that is, 0.035.

$$\ln r_{s25_sap} = -0.1 \times (T_5 - 25) + C \quad (31)$$

We obtained the m_{sap} by above-ground biomass and allometric functions. First, A_{stem} was expressed as a function of stem biomass (m_{stem}) and the allometric parameters c and d, two relatively conservative parameters generated using measurements from BAAD (*43*),

$$A_{stem} = c \times m_{stem}^{d} \quad (32)$$

Assuming equal densities of sapwood and overall stem woody tissue, we can likewise express the sapwood biomass by considering Eqs. 2-3 as follows,

$$m_{sap} = m_{stem} \times \frac{n}{(n-1) \times b_0 + 1} \times \frac{A_{sap}}{A_{stem}} \quad (33)$$

By expressing A_{sap} and A_{stem} in dependence of m_{stem} (Eq. 1 and 30), we can obtain,

$$m_{sap} = \frac{n}{(n-1) \times b_0 + 1} \times a_0 \times c^{b_0 - 1} \times m_{stem}^{(b_0 - 1) \times d + 1} \quad (34)$$

We then expressed the Eq. 30 further by the following equation,

$$F_s = \sum_{i=1}^{n} r_{s25_sap} \times f(T) \times \frac{n}{(n-1)\times b_0 + 1} \times a \times c^{b_0 - 1} \times m_{stem}^{(b_0-1)\times d+1} \times Area \times Time_{growth} \quad (35)$$

where n describes the shape of the tree stem, assumed as a mean value of 2.5. The allometric parameters a_0, b_0, c and d were caculated using measurements contained in BAAD, which represent mean value of 0.365, 0.877, 0.0008 and 0.748 (*43*), respectively.

3.2.2 Simulation of stem respiration in 2010, as an example

We applied the simple model shown above (Eq. 35) to estimate stem respiration at global scale, using above-ground biomass data from 2010 from the GBDP, and daily mean temperature from CRU TS version 4.02. All data were standardized to a spatial resolution of 0.5º to run the model. The global CO_2 emission was calculated through summation. We used quadratic mean values to calculate the standard error (SE) of stem respiration, following the law of propagation of uncertainty (SI section 3.2.3). And our final estimate of the annual CO_2 released by stem respiration globally was 18.8±5.9Pg C (Fig. 4A). The distribution range of global simulation is determined based on the distribution range of above-ground biomass from GBDP, which is the mass, expressed as oven-dry weight of the woody parts (stem, bark, branches and twigs) of all living trees excluding stump and roots (*42*).

We further extracted the distribution of forests to calculate global simulation from forest only area. We extracted forest land cover information from the Moderate Resolution Imaging Spectroradiometer (MODIS) land cover product (MCD12C1) in 2010 (*101*). The original 0.05º×0.05º (longitude×latitude) resolution grid was aggregated to 0.5º×0.5º by majority vote method. By using the forest range as the cropping layer, we obtain the estimate of F_s from forest only area globally is about 10.5±3.2 PgC.

3.2.3 Uncertainty in global simulation

During the process of simulation, we calculated various sources of uncertainty. Uncertainty in modelled R_s derived from GBDP biomass, from the calibration of basal r_{s25}, from Q_{10} value and allometric parameters. The standard error of r_{s25} and Q_{10} were 0.035 (table S10) and 0.2 (*65*). We used the square root of the variance of the residuals from the fitted allometric models to calculate standard error of a_0, b_0, c and d (0.051, 0.029, 0.0001 and 0.019, respectively) *(43)*. The GBDP biomass data has a standard error per grid cell provided by GBDP; this introduced the most uncertainty.

$$SE_{R_s} = \sqrt{SE_{AGB}^2 + SE_{r_{s25}}^2 + SE_{Q_{10}}^2 + SE_{(a,b)}^2 + SE_{(c,d)}^2} \quad (36)$$

3.2.4 Global estimate of stem respiration from TRENDY

We compared our EEO-based global stem respiration in 2010 with estimates from nine TRENDY models (version 9, 2021, scenario 2) (*118*). TRENDY does not directly report stem respiration (R_s), so we approximated it by adjusting reported values of autotrophic respiration (R_a) to remove the contribution of leaf respiration (R_{leaf}) and root respiration. To do so, we used information on the vegetation and root carbon pools, and an assumption of leaf respiration as a fraction of *GPP* (Equation below):

$$R_s = R_{shoot} - R_{leaf} = R_a \times \frac{(cVeg - cRoot)}{cVeg} - c \times GPP \quad (37)$$

We estimated leaf respiration to be a constant portion, c, of 25-35% of annual GPP, based on estimates from previous studies (*13, 44, 131, 132*). This conservative range was used in order to quantify

uncertainties in stem respiration estimates from TRENDY models resulting from the assumption of a fractional contribution from *GPP* (fig. S7). We utilized a mass-based approach to convert total autotropic respiration to aboveground autotropic respiration, by multiplying R_a with the vegetation biomass fraction allocated to aboveground biomass ((cVeg-cRoot)/cVeg). We further inferred the ratio of R_{stem} to R_a by dividing the obtained R_{stem} by R_a estimations reported by each TRENDY model.

3.2.5 Simulation of future stem respiration under different scenarios

To estimate the effect of considering the thermal acclimation of stem respiration, we calculated the carbon emission reduction over the period 2015-2100 with and without introducing acclimation (F_s), using outputs from four models and two scenarios. The reduction caused by considering thermal acclimation ($F_{s.re}$) can be expressed as follows

$$F_{s.re} = \sum_{i=1}^{n} \left[\left(r_{s25_sap} - r_{n_sap} \right) \times f\left(T\right) \times m_{sap} \times Area \times Time_{growth} \right] \quad (38)$$

where $F_{s.re}$ represents the carbon emission reduction compared to non-acclimated respiration in each year. r_{s25_sap} is the reference sapwood mass-based stem respiration calculated by the model. r_{n_sap} is the reference sapwood mass-based stem respiration from the modern parameter calibration and is kept constant in simulations. The temperature used to calculate r_{n_sap}, $f(T)$ and $Time_{growth}$ was extracted from CMIP6 models (SI section 1.6).

We have checked the algorithms used on the state-of-the-art Land Surface Models. Most Land Surface Models, such as ORCHIDEE (*24*) and JULES (*26*), have not yet considered the acclimation of stem respiration. A few Land Surface Models, such as CABLE (*27*) and QUINCY (*29*), have considered the thermal acclimation of stem respiration but they apply the same algorithm as that used by CLM5, i.e. they treat respiration acclimation in stems the same way as that in leaves.In those models, r_{s25} is predicted to decrease with temperature by 1.83 % K^{-1}, adopting the same thermal acclimation hypothesis by Atkin et al. (*40*). We therefore used CLM5 as the example for this comparison, by taking the algorithm used in CLM5 from its code (https://github.com/ESCOMP/CTSM), which takes thermal acclimation into account as follows

$$r_{s25_clm5} = r \times 10^{\left[-0.00794 \times (T_5 - 25)\right]} \quad (39)$$

where r_{s25_clm5} means reference stem respiration considering thermal acclimation, r is a PFT-specific parameter (*28*). The natural-log stem respiration in CLM5 decreases with temperature by 1.83 % K–1, about 18% of our theoretical prediction. We then applied Eq. 40 to replace r_{s25_sap} in Eq. 39, using temperature extracted from CLM5 outputs in the future SSP126 and SSP585 scenarios. It would result in a release of *ca.* 5.4 and 13.9 PgC additional CO_2 by 2100 compared to our simulations.

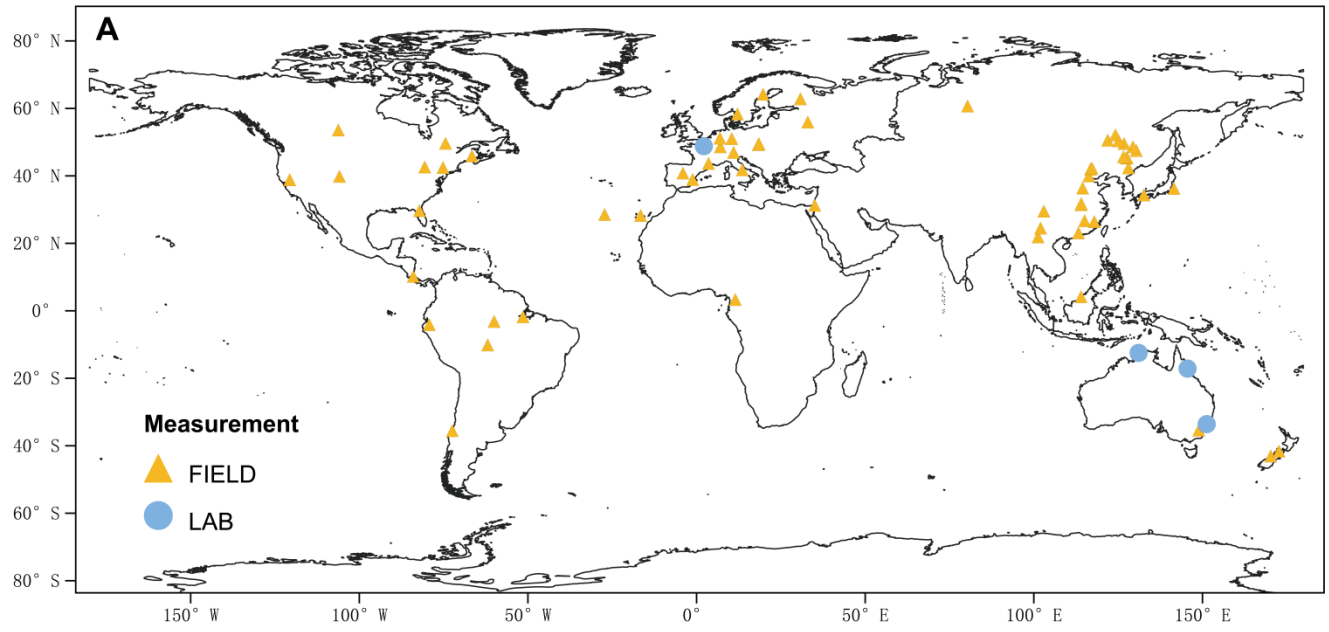

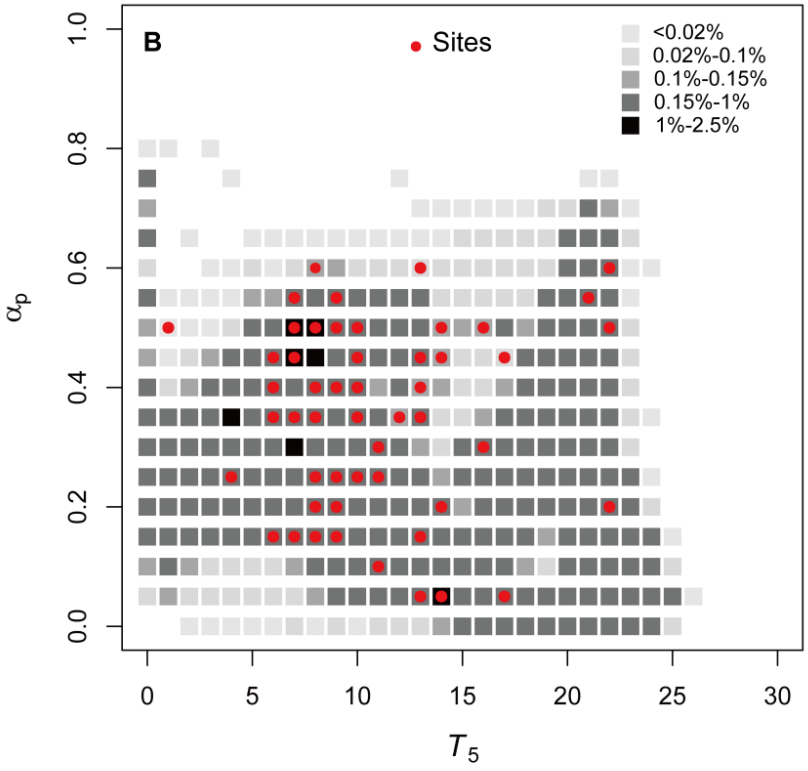

fig. S1. Sites. fig. S1A shows the location of sites used for field (orange triangle) and laboratory (blue circle) measurements of stem respiration. fig. S1B plots show the location of the samples (red points) in climate space, defined by α_p (AET/PET) and the mean value of the excess temperature above 5 °C (T_5). The gray shading indicates the frequency of each climate globally.

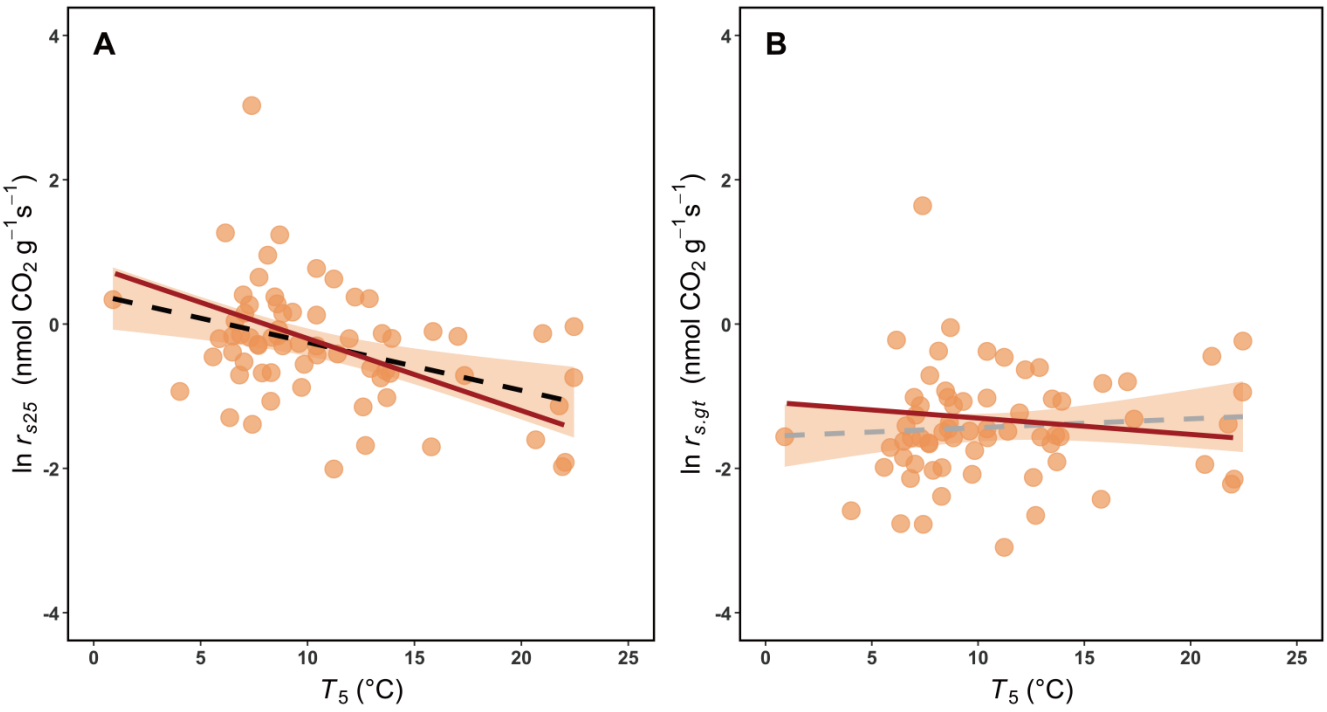

fig. S2. Relationships between natural log-transformed values of site-mean stem respiration and growth temperature. r_{s25} and $r_{s.gt}$ represent stem respiration rate standardized to the reference temperature of 25°C and the mean value of the excess temperature above 5°C (T_5), respectively. The orange dots represent the site-means of r_{s25} and $r_{s.gt}$ calculated as the averaged value of all individual measurements in each site. The dashed lines are the data-fitted regression lines (black: significant slope; gray: non-significant slope) whereas the shaded areas represent the 95% confidence intervals. The solid red lines represent the theoretical predictions. Mathematical details are provided in table S5.

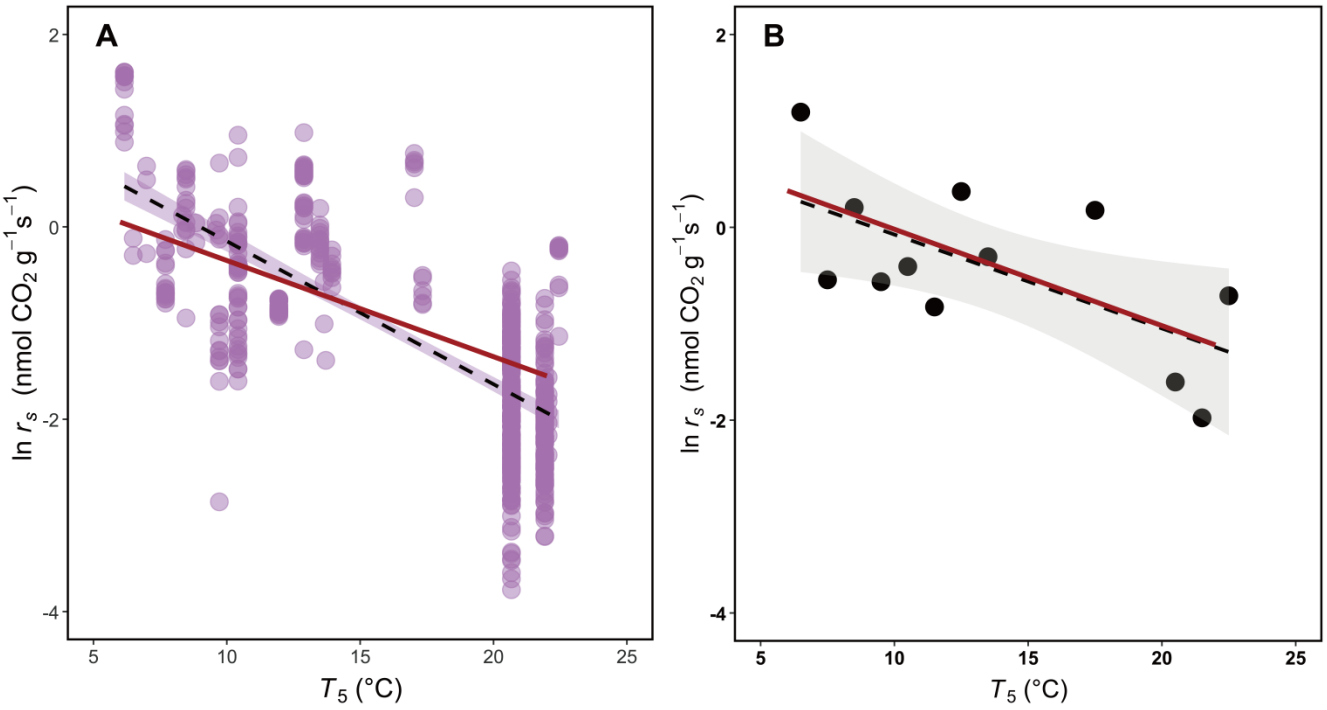

fig. S3. Relationships between natural log-transformed values of stem respiration and growth temperature based on samples with no temperature standardization. r_s represents stem respiration rate whose measuring temperature was within 1 ℃ of 25 ℃ (from 24 to 26℃). fig. S3A displays the raw data, while fig. S3B shows the data after dividing T_5 into 20 bins and calculating mean r_s value within each bin. The black dashed lines represent the linear fitting line. The shaded areas represent the 95% confidence intervals. The solid red lines represent the theoretical predictions of thermal sensitivity. Mathematical details are provided in table S6.

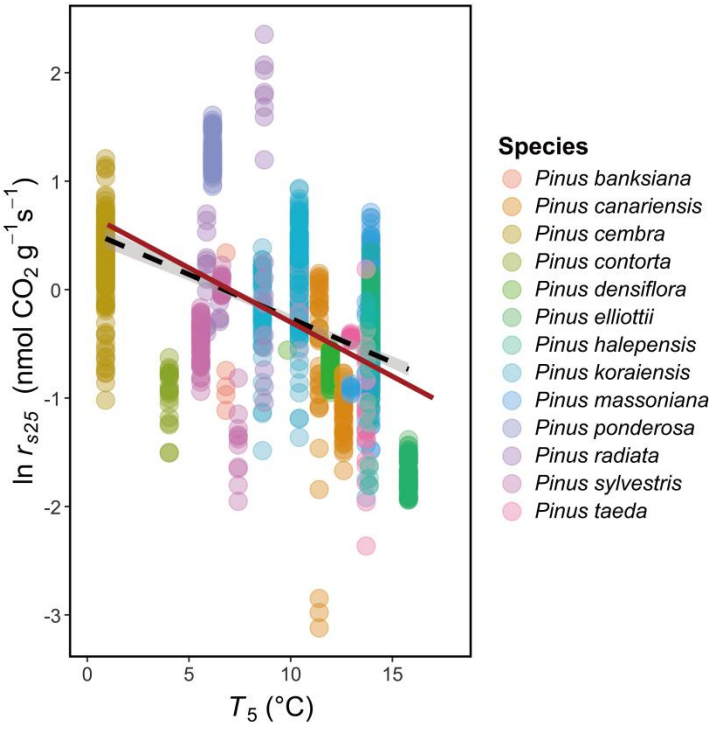

1085

1086 **fig. S4. Relationships between natural log-transformed values of stem respiration and growth**
1087 **temperature based on samples of *Pinus*.** r_{s25} represents the stem respiration rate standardized to the
1088 reference temperature of 25℃, and T_5 is the mean value of the excess temperature above 5℃. Different
1089 colors represent different species within the genus *Pinus*. The black dashed line is the linear fitting line.
1090 The shaded area represents the 95% confidence intervals. The solid red line is the theoretical prediction
1091 of thermal sensitivity. Mathematical details are provided in table S9.

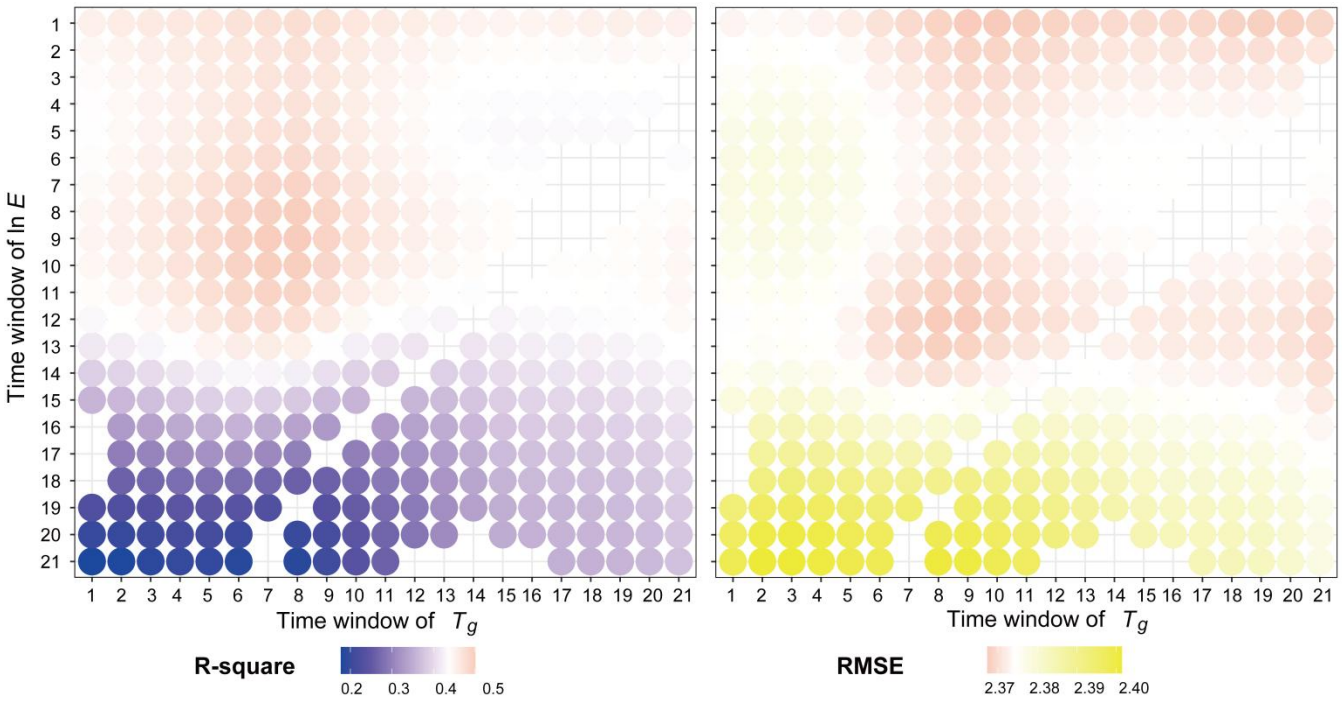

fig. S5. R-square and RMSE of multiple regression between natural log-transformed values of stem respiration, growth temperature and transpiration across various time scales. The figures show the R-square and root mean square error (RMSE) values from multiple regression analysis between lnr_{s25}, T_g and ln$E$. r_{s25} represents the stem respiration rate standardized to the reference temperature of 25℃. T_g and ln$E$ are the mean growing temperature and natural log-transformed transpiration across various time scales. The horizontal axis represents different time scales for T_g, ranging from 1 day to 21 days, indicating the average temperature over the 1-21 days prior to stem respiration measurements. The vertical axis depicts various time scales for ln$E$, also spanning from 1 day to 21 days. The different colors indicate the magnitude of the R-square and RMSE values.

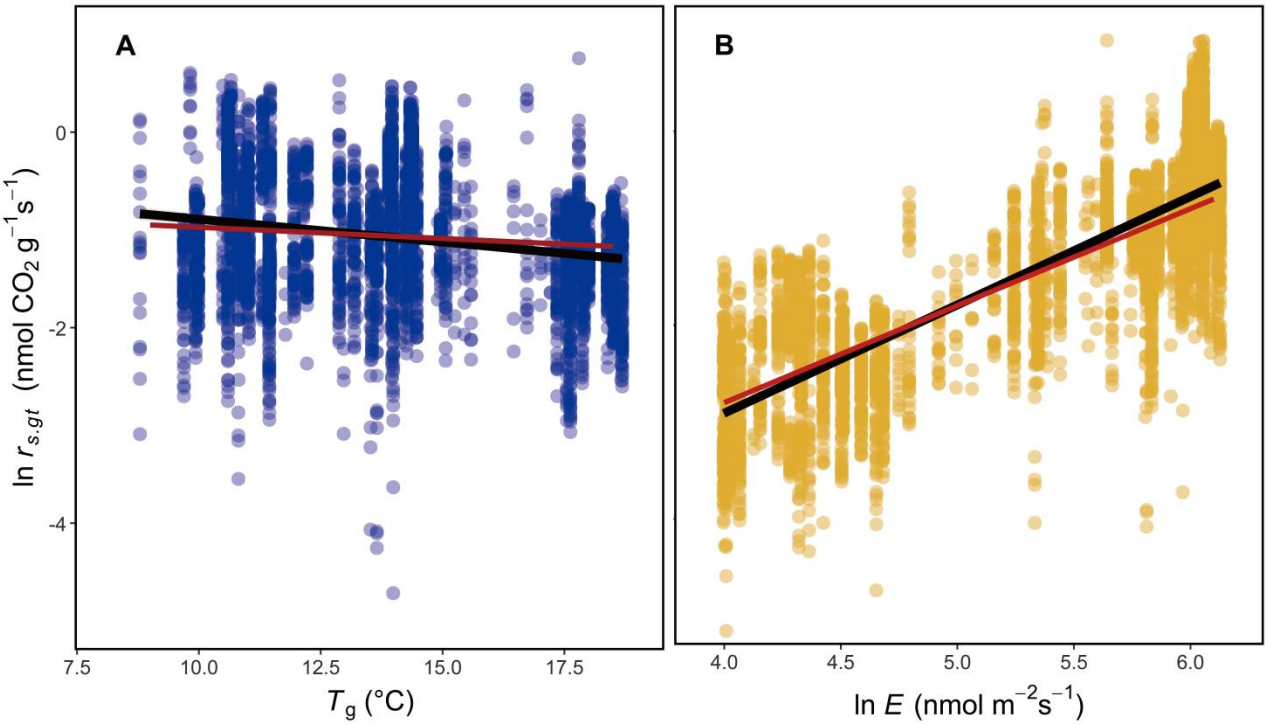

fig. S6. Partial residual plots showing the relationship between stem respiration and (a) temperature and (b) transpiration when other factors are held constant. (A) Growth temperature (*Tg*) is an average of the six days before stem respiration was measured. $r_{s.gt}$ is stem respiration, natural-log transformed, at growth temperature (T_g). **(B)** Transpiration (E) is an average of the thirteen days before measurement and was natural-log transformed. The solid black lines represent the relationship fitted via multiple regression ($\ln r_{s25} = (-0.047\pm0.005)\times T_g + (1.117\pm0.018)\times \ln E$, $R^2=0.60$, $p<0.001$, VIF=2.01). The red solid lines represent the theoretical prediction, with coefficients of −0.023 and 1 for temperature and ln transpiration, respectively.

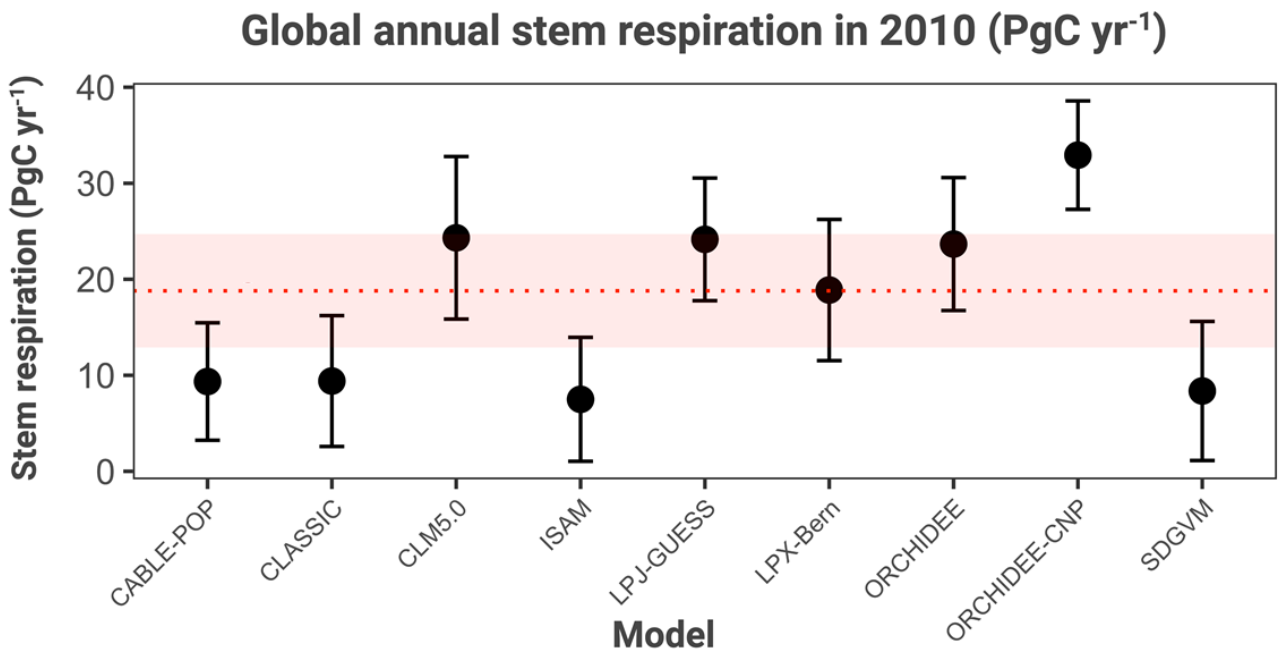

fig. S7. Estimate of stem respiration from TRENDY models. A comparison between global annual stem respiration in 2010 derived in this study (red) and that obtained from 9 models included in the TRENDY model ensemble (black). See supplementary section 3.2.4 for more information on how stem respiration is estimated from the TRENDY models.

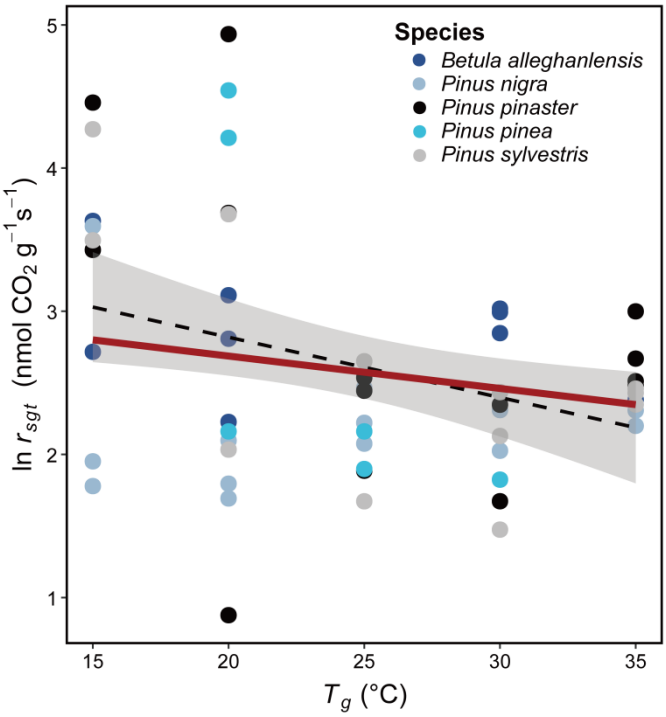

fig. S8. Relationship between $r_{s.gt}$ and growing temperature from a warming experiment. $r_{s.gt}$ represents stem respiration standardized to the growing temperature (T_g). Growth temperature (T_g) is the temperature at which individual species were grown. Points with different colors represent different species. The dashed line was fitted ($\ln r_{s25} = (-0.047 \pm 0.005) \times T_g$, $R^2=0.10$) using linear regression analysis by all samples. The shaded area represents the 95% confidence intervals. The original data are from warming experiment Smith et al., 2016 included in GSRD.

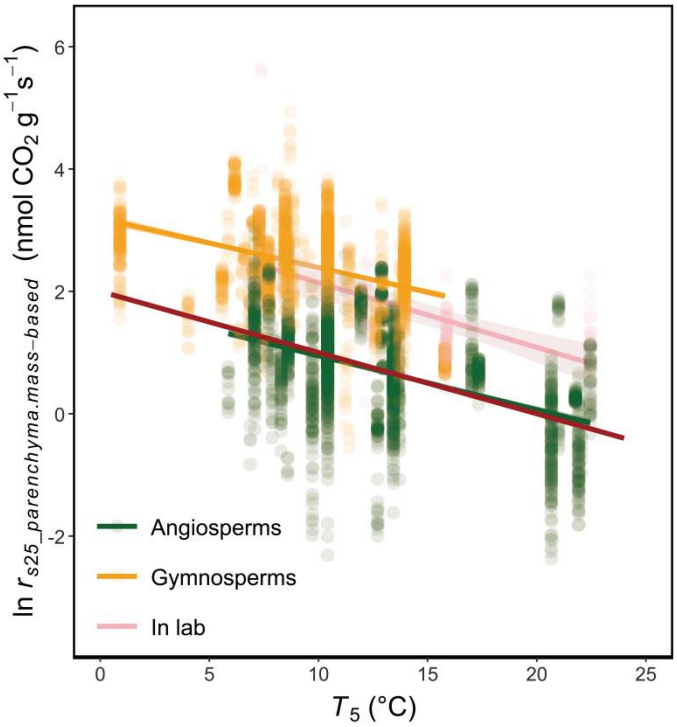

fig. S9. Global trends of natural log-transformed stem respiration at reference temperature (r_{s25}) in relation to the mean value of the excess temperature above 5 °C (T_5) using parenchyma mass-based value. Stem respiration was measured in the laboratory (pink circles) and in the field (orange circles for Gymnosperm, green circles for Angiosperm). $r_{s25_parenchyma_mass\text{-}based}$ represents stem respiration standardized to the reference temperature of 25 °C, and T_5 is the mean value of the excess temperature above 5°C. Solid fitted lines are shown for the Gymnosperm (green line), Angiosperm (orange line) and in lab data (pink line) separately (Mathematical details are provided in table S14). The shaded area represents the 95% confidence intervals. The solid red line is the theoretical prediction of thermal sensitivity, whose slope is −10.1% K^{-1}.

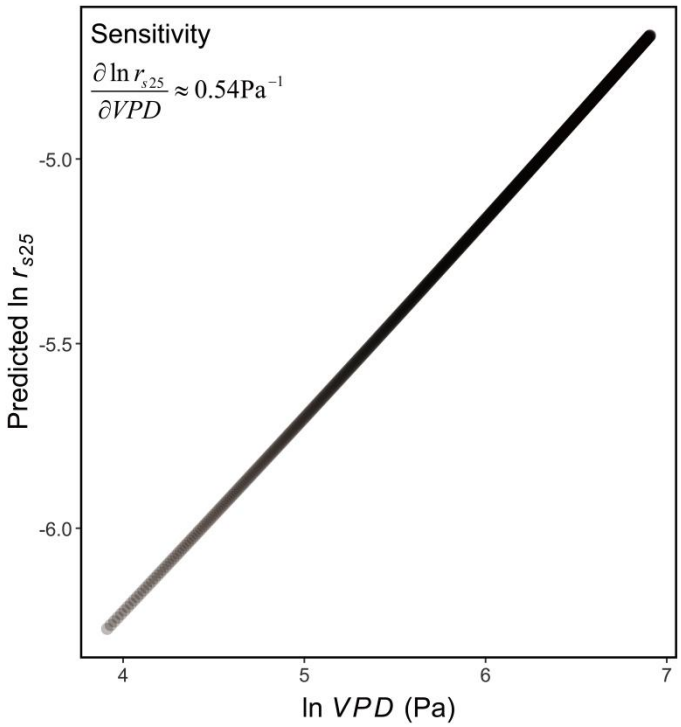

fig. S10. Theoretical prediction of vapor pressure deficit effect on the natural log-transformed stem respiration rate standardized to a reference temperature of 25℃ (lnr_{s25}). Sensitivity analysis of natural-log r_{s25} to natural-log *VPD*, by setting the temperature as 25°C, atmosphere pressure as 101325 Pa, *fAPAR* as 1, *PPFD* as 300 mol m^{-2} $month^{-1}$ and *VPD* from 50 to 1000 Pa. All else equal, lnr_{s25} has a nearly linear relationship with ln*VPD*, with a sensitivity of −0.54 Pa^{-1}.

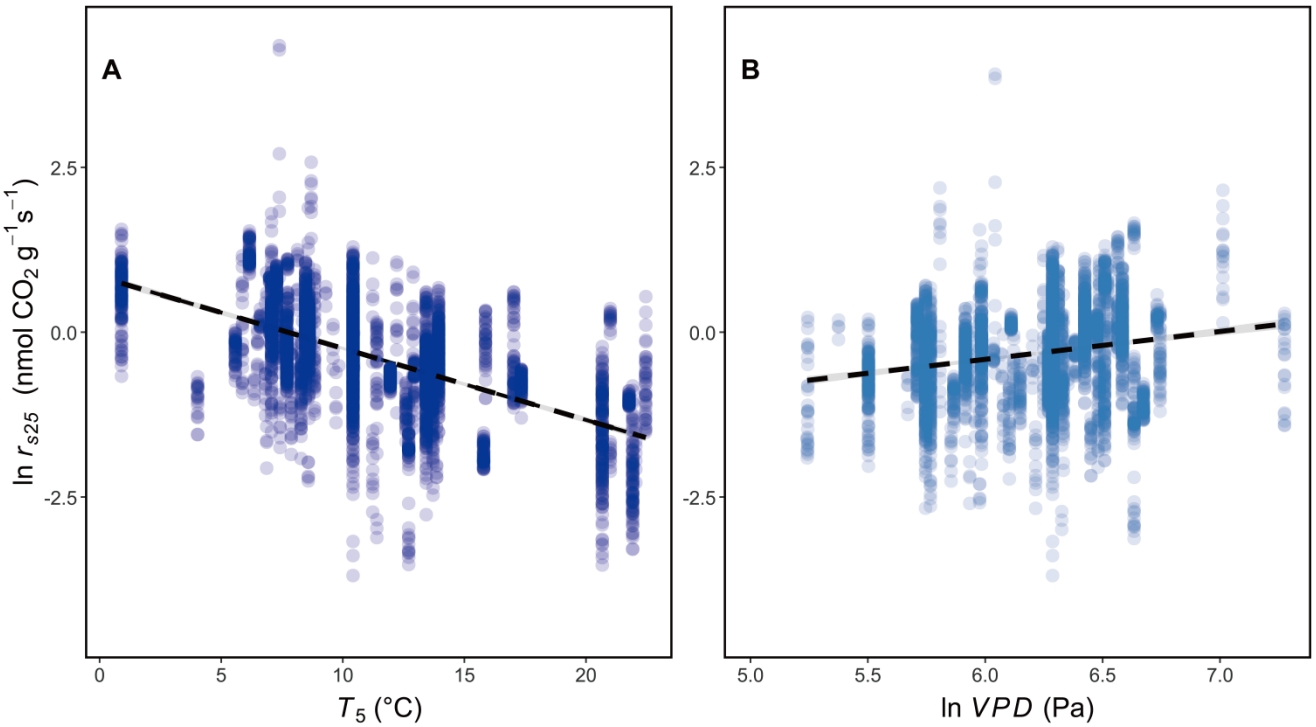

fig. S11. Partial residual plots showing the relationship between stem respiration and vapor pressure deficit and temperature when other factors are held constant. r_{s25} represents the stem respiration standardized to the reference temperature of 25℃, *VPD* (Pa) is vapor pressure deficit in sites, and T_5 (℃) is the mean value of the excess temperature above 5℃. The black dashed line is the linear fitting line. The shaded area represents the 95% confidence intervals. Mathematical details are provided in tableS15.

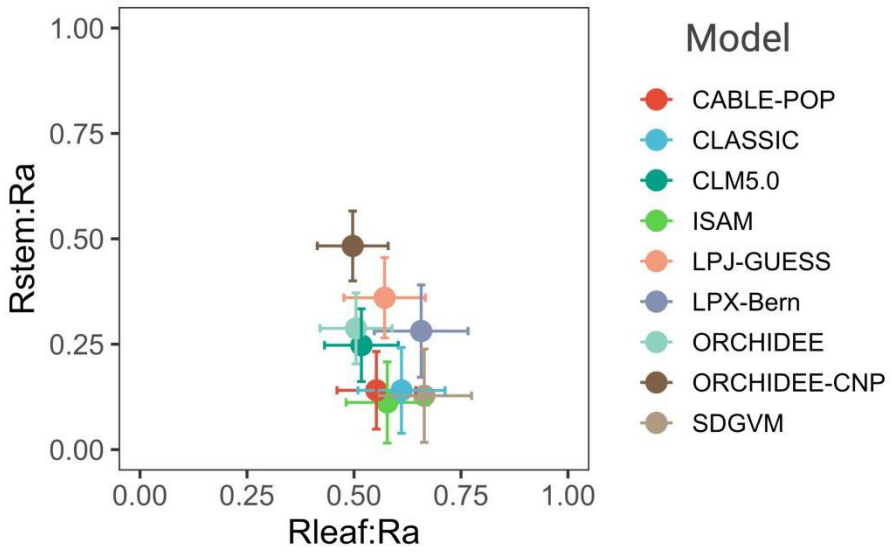

fig. S12. Estimate of the ratio of leaf or stem respiration to total autotrophic respiration from TRENDY models. We inferred the ratio of R_{stem} (or R_{leaf}) to R_a by dividing the obtained R_{stem} (or R_{leaf}) by R_a estimations reported by each TRENDY model. See supplementary section 3.2.4 for detailed information on how stem respiration is estimated from the TRENDY models.

Criterion	Details
Age	Measurements on adult trees, using a minimum diameter of 10 centimeters to exclude saplings, except for warming experiment data from Smith et al., 2019.
Species/Size	Only used records that provide the name of the species of measurement values. In-field measurement must have diameter information for samples or mean diameter of tree trunk at breast height for all observations.
Time of the year	Measurements taken within the growing season. In sites with a dry and wet season, the measurements were made in the wet season. The growing season and wet season were defined by each specific researcher.
Measuring Height	Measurements of stem respiration were made at or near breast height (about 1.5 meters above the ground) to exclude vertical variation.
Orientation	Measurements at a given site were made on the same side of the tree trunk to avoid the impact of different trunk orientations on respiration rate.
Control factors	Measurements were made on woody plants in their natural growth state, without human control factors such as soil nutrient gradients, carbon dioxide fertilization, bark girdling, sparse forests and so on.
Temperature	References need to provide the temperature when the respiration was measured to allow standardization to a reference temperature.

table S1. Criteria of data filtering for Global Stem Respiration Dataset.

LON	LAT	CLIMATE ZONE	PFT	REF	MEAS	FINAL_SPNAME	AUTHORITY	OBS NUM
−66.6	45.95	Boreal	Evergreen needles	Lavigne et al., 2004	FIELD	*Abies balsamea*	(L.) Mill.	9
103	29.57	Temperate	Evergreen needles	Zhao et al., 2018	FIELD	*Abies fabri*	(Mast.) Craib	4
131.11	−12.46	Tropical	Evergreen Broadleaf	Westerband et al., 2022	LAB	*Acacia difficilis*	Maiden	1
131.11	−12.46	Tropical	Evergreen Broadleaf	Westerband et al., 2022	LAB	*Acacia latescens*	Benth.	1
131.11	−12.46	Tropical	Evergreen Broadleaf	Westerband et al., 2022	LAB	*Acacia mimula*	Pedley	1
151.29	−33.58	Temperate	Evergreen Broadleaf	Westerband et al., 2022	LAB	*Acacia suaveolens*	(Sm.) Willd.	1
127.53	45.38	Boreal	Deciduous Broadleaf	Yang et al., 2012	FIELD	*Acer pictum*	Maxim.	56
−75.17	42.5	Temperate	Deciduous Broadleaf	Reinmann et al., 2015	FIELD	*Acer rubrum*	L.	20
−66.6	45.95	Boreal	Deciduous broadleaf	Lavigne et al., 2004	FIELD	*Acer rubrum*	L.	6
145.62	−17.12	Tropical	Evergreen Broadleaf	Westerband et al., 2022	LAB	*Acronychia acidula*	F.Muell.	1
145.62	−17.12	Tropical	Evergreen Broadleaf	Westerband et al., 2022	LAB	*Acronychia laevis*	J.R.Forst. & G.Forst.	1
145.62	−17.12	Tropical	Evergreen needles	Westerband et al., 2022	LAB	*Agathis robusta*	(C.Moore ex F.Muell.) F.M.Bailey	1
145.62	−17.12	Tropical	Evergreen Broadleaf	Westerband et al., 2022	LAB	*Aleurites rockinghamensis*	(Baill.) P.I.Forst.	1
145.62	−17.12	Tropical	Evergreen Broadleaf	Westerband et al., 2022	LAB	*Alphitonia petriei*	Braid & C.T.White	1
145.62	−17.12	Tropical	Evergreen Broadleaf	Westerband et al., 2022	LAB	*Alphitonia whitei*	Braid	1
145.62	−17.12	Tropical	Evergreen Broadleaf	Westerband et al., 2022	LAB	*Alstonia muelleriana*	Domin	1
145.62	−17.12	Tropical	Evergreen Broadleaf	Westerband et al., 2022	LAB	*Alstonia scholaris*	(L.) R.Br.	1
−51.45	−1.72	Tropical	Evergreen Broadleaf	Rowland et al., 2018	FIELD	*Aspidosperma*	Mart.	1
−51.45	−1.72	Tropical	Evergreen Broadleaf	Rowland et al., 2018	FIELD	*Aspidosperma araracanga*	Marc.-Ferr.	1

−51.45	−1.72	Tropical	Evergreen Broadleaf	Rowland et al., 2018	FIELD	*Aspidosperma desmanthum*	Benth. ex Müll.Arg.	1
−51.45	−1.72	Tropical	Evergreen Broadleaf	Rowland et al., 2018	FIELD	*Aspidosperma nitidum*	Benth. ex Müll.Arg.	1
101.27	21.93	Temperate	Evergreen Broadleaf	Yan et al., 2009	FIELD	*Barringtonia macrostachya*	Kurz	24
117.95	26.47	Temperate	Evergreen Broadleaf	Wei et al., 2009	FIELD	*Bauhinia purpurea*	L.	24
145.62	−17.12	Tropical	Evergreen Broadleaf	Westerband et al., 2022	LAB	*Beilschmiedia bancroftii*	(F.M.Bailey) C.T.White	1
6.95	51.23	Boreal	Deciduous broadleaf	Gansert et al., 2005	FIELD	*Betula pendula*	Roth	35
126.63	45.72	Boreal	Deciduous Broadleaf	Wang et al., 2011	FIELD	*Betula platyphylla*	Sukaczev	2
127.53	45.38	Boreal	Deciduous Broadleaf	Yang et al., 2012	FIELD	*Betula platyphylla*	Sukaczev	52
127.67	45.4	Boreal	Deciduous broadleaf	Dou et al., 2011	FIELD	*Betula platyphylla*	Sukaczev	9
127.67	45.4	Boreal	Deciduous broadleaf	Shi et al., 2010	FIELD	*Betula platyphylla*	Sukaczev	54
131.11	−12.46	Tropical	Evergreen Broadleaf	Westerband et al., 2022	LAB	*Buchanania obovata*	Engl.	1
151.29	−33.58	Temperate	Evergreen Broadleaf	Westerband et al., 2022	LAB	*Callistemon salignus*	Craven	1
145.62	−17.12	Tropical	Evergreen Broadleaf	Westerband et al., 2022	LAB	*Cardwellia sublimis*	F.Muell.	1
102.03	24.53	Temperate	Evergreen Broadleaf	Hu et al., 2010	FIELD	*Castanopsis rufescens*	(Hook.f.?& Th.)?C.C.Huang?&?Y.T.Chang	6
145.62	−17.12	Tropical	Evergreen Broadleaf	Westerband et al., 2022	LAB	*Castanospermum australe*	A.Cunn & C.Fraser	1
145.62	−17.12	Tropical	Evergreen Broadleaf	Westerband et al., 2022	LAB	*Castanospora alphandi*	(F.Muell.) F.Muell.	1
151.29	−33.58	Temperate	Evergreen Broadleaf	Westerband et al., 2022	LAB	*Casuarina glauca*	Spreng.	1
141.58	36.32	Temperate	Evergreen needles	Araki et al., 2015	FIELD	*Chamaecyparis obtusa*	(Siebold & Zucc.) Endl.	12
−51.45	−1.72	Tropical	Evergreen Broadleaf	Rowland et al., 2018	FIELD	*Chrysophyllum manaosense*	(Aubrév.) T.D.Penn.	1
117.95	26.47	Temperate	Evergreen Broadleaf	Wei et al., 2009	FIELD	*Cinnamomum camphora*	(L.) J.Presl	24

145.62	−17.12	Tropical	Evergreen Broadleaf	Westerband et al., 2022	LAB	*Cinnamomum laubatii*	F.Muell.	1
145.62	−17.12	Tropical	Evergreen Broadleaf	Westerband et al., 2022	LAB	*Cleistanthus semiopacus*	?F.Muell. ex Benth.	1
−79.25	−4.06	Tropical	Evergreen Broadleaf	Zach et al., 2010	FIELD	*Clethra revoluta*	(Ruiz & Pav.) Spreng.	71
131.11	−12.46	Tropical	Evergreen Broadleaf	Westerband et al., 2022	LAB	*Corymbia bleeseri*	(Blakely) K.D.Hill & L.A.S.Johnson	1
151.29	−33.58	Temperate	Evergreen Broadleaf	Westerband et al., 2022	LAB	*Corymbia gummifera*	(Gaertn.) K.D.Hill & L.A.S.Johnson	1
151.29	−33.58	Temperate	Evergreen Broadleaf	Westerband et al., 2022	LAB	*Corymbia maculata*	(Hook.) K.D.Hill & L.A.S.Johnson	1
131.11	−12.46	Tropical	Evergreen Broadleaf	Westerband et al., 2022	LAB	*Corymbia porrecta*	(S.T.Blake) K.D.Hill & L.A.S.Johnson	1
145.62	−17.12	Tropical	Evergreen Broadleaf	Westerband et al., 2022	LAB	*Croton bernierus*	(Bailey)?Edlin? ex J.H.Boas	1
145.62	−17.12	Tropical	Evergreen Broadleaf	Westerband et al., 2022	LAB	*Croton insularis*	Baill.	1
145.62	−17.12	Tropical	Evergreen Broadleaf	Westerband et al., 2022	LAB	*Cryptocarya mackinnoniana*	F.Muell.	1
145.62	−17.12	Tropical	Evergreen Broadleaf	Westerband et al., 2022	LAB	*Cryptocarya murrayi*	F.Muell.	1
117.95	26.47	Temperate	Evergreen needles	Wei et al., 2009	FIELD	*Cunninghamia lanceolata*	(Lamb.) Hook.	24
170.3	−43	Temperate	Evergreen needles	Bowman et al., 2005	FIELD	*Dacrydium cupressinum*	Sol. ex G.Forst.	6
145.62	−17.12	Tropical	Evergreen Broadleaf	Westerband et al., 2022	LAB	*Daphnandra repandula*	(F.Muell.) F.Muell.	1
145.62	−17.12	Tropical	Evergreen Broadleaf	Westerband et al., 2022	LAB	*Darlingia darlingiana*	(F.Muell.) L.A.S.Johnson	1
145.62	−17.12	Tropical	Evergreen Broadleaf	Westerband et al., 2022	LAB	*Dendrocnide photiniphylla*	(Kunth) Chew	1
145.62	−17.12	Tropical	Evergreen Broadleaf	Westerband et al., 2022	LAB	*Dinosperma erythrococca*	(F.Muell.) T.G.Hartley	1
11.5	3.38	Tropical	Evergreen Broadleaf	Meir et al., 2019	FIELD	*Distemonanthus benthamianus*	Baill.	28
114.03	4.2	Tropical	Evergreen	Katayama et al., 2014	FIELD	*Dryobalanops*	C.F.Gaertn.	4

			Broadleaf			*sumatrensis*		
145.62	−17.12	Tropical	Evergreen Broadleaf	Westerband et al., 2022	LAB	*Elaeocarpus angustifolius*	F.Muell.	1
145.62	−17.12	Tropical	Evergreen Broadleaf	Westerband et al., 2022	LAB	*Endiandra monothyra*	B.Hyland	1
−79.25	−4.06	Tropical	Evergreen Broadleaf	Zach et al., 2010	FIELD	*Endlicheria oreocola*	Chanderb.	56
151.29	−33.58	Temperate	Evergreen Broadleaf	Westerband et al., 2022	LAB	*Eriostemon australasius*	Pers.	1
131.11	−12.46	Tropical	Evergreen Broadleaf	Westerband et al., 2022	LAB	*Erythrophleum chlorostachys*	(F.Muell.) Baill.	1
−51.45	−1.72	Tropical	Evergreen Broadleaf	Rowland et al., 2018	FIELD	*Eschweilera coriacea*	(DC.) S.A.Mori	2
−51.45	−1.72	Tropical	Evergreen Broadleaf	Rowland et al., 2018	FIELD	*Eschweilera grandiflora*	(Aubl.) Sandwith	5
151.29	−33.58	Temperate	Evergreen Broadleaf	Westerband et al., 2022	LAB	*Eucalyptus haemastoma*	Sm.	1
131.11	−12.46	Tropical	Evergreen Broadleaf	Westerband et al., 2022	LAB	*Eucalyptus miniata*	A.Cunn. Ex Schauer	1
151.29	−33.58	Temperate	Evergreen Broadleaf	Westerband et al., 2022	LAB	*Eucalyptus racemosa*	Cav.	1
150.74	−33.62	Temperate	Evergreen Broadleaf	Noh et al., 2021	FIELD	*Eucalyptus tereticornis*	Sm.	5
150.74	−33.62	Temperate	Evergreen Broadleaf	Salomon et al., 2019	FIELD	*Eucalyptus tereticornis*	Sm.	119
131.11	−12.46	Tropical	Evergreen Broadleaf	Westerband et al., 2022	LAB	*Eucalyptus tetrodonta*	F.Muell.	1
2.17	48.83	Boreal	Deciduous broadleaf	Demasin, 2003	LAB	*Fagus sylvatica*	L.	8
7.07	48.67	Boreal	Deciduous broadleaf	Ceschia et al., 2002	FIELD	*Fagus sylvatica*	L.	9
10.45	51.08	Boreal	Deciduous broadleaf	Ostrowski, 2007	FIELD	*Fagus sylvatica*	L.	172
13.58	41.85	Temperate	Deciduous broadleaf	Guidolotii et al., 2013	FIELD	*Fagus sylvatica*	L.	27
117.95	26.47	Temperate	Evergreen Broadleaf	Wei et al., 2009	FIELD	*Ficus altissima*	Blume	24
145.62	−17.12	Tropical	Evergreen Broadleaf	Westerband et al., 2022	LAB	*Flindersia bourjotiana*	F.Muell.	1
145.62	−17.12	Tropical	Evergreen Broadleaf	Westerband et al., 2022	LAB	*Flindersia brayleyana*	F.Muell.	1

145.62	−17.12	Tropical	Evergreen Broadleaf	Westerband et al., 2022	LAB	*Flindersia pimenteliana*	F.Muell.	1
145.62	−17.12	Tropical	Deciduous broadleaf	Westerband et al., 2022	LAB	*Franciscodendron laurifolium*	(F.Muell.) B.Hyland & Steenis	1
−66.6	45.95	Boreal	Deciduous broadleaf	Lavigne et al., 2004	FIELD	*Fraxinus americana*	L.	8
126.63	45.72	Boreal	Deciduous Broadleaf	Wang et al., 2011	FIELD	*Fraxinus mandshurica*	Rupr.	2
127.53	45.38	Boreal	Deciduous Broadleaf	Yang et al., 2012	FIELD	*Fraxinus mandshurica*	Rupr.	62
127.67	45.4	Boreal	Deciduous broadleaf	Shi et al., 2010	FIELD	*Fraxinus mandshurica*	Rupr.	53
128.1	42.4	Temperate	Deciduous broadleaf	Wang et al., 2005	FIELD	*Fraxinus mandshurica*	Rupr.	45
145.62	−17.12	Tropical	Evergreen Broadleaf	Westerband et al., 2022	LAB	*Gillbeea adenopetala*	F.Muell.	1
145.62	−17.12	Tropical	Evergreen Broadleaf	Westerband et al., 2022	LAB	*Gossia hillii*	(Benth.) N.Snow & Guymer	1
−51.45	−1.72	Tropical	Evergreen Broadleaf	Rowland et al., 2018	FIELD	*Goupia glabra*	Aubl.	1
−79.25	−4.06	Tropical	Evergreen Broadleaf	Zach et al., 2010	FIELD	*Graffenrieda emarginata*	Triana	60
131.11	−12.46	Tropical	Evergreen Broadleaf	Westerband et al., 2022	LAB	*Grevillea decurrens*	Ewart	1
131.11	−12.46	Tropical	Evergreen Broadleaf	Westerband et al., 2022	LAB	*Grevillea pteridifolia*	Knight	1
151.29	−33.58	Temperate	Evergreen Broadleaf	Westerband et al., 2022	LAB	*Grevillea speciosa*	(Knight) McGill.	1
151.29	−33.58	Temperate	Evergreen Broadleaf	Westerband et al., 2022	LAB	*Hakea dactyloides*	Cav.	1
151.29	−33.58	Temperate	Evergreen Broadleaf	Westerband et al., 2022	LAB	*Hakea pugioniformis*	Britten	1
101.27	21.93	Temperate	Evergreen Broadleaf	Yan et al., 2009	FIELD	*Hevea brasiliensis*	(Willd. ex A.Juss.) Müll.Arg.	24
−84	10.26	Tropical	Evergreen Broadleaf	Asao et al., 2015	FIELD	*Hieronyma alchorneoides*	Allem?o	59
145.62	−17.12	Tropical	Evergreen Broadleaf	Westerband et al., 2022	LAB	*Homalium circumpinnatum*	F.M.Bailey	1

−60.02	−3.12	Tropical	Evergreen Broadleaf	Kunert et al., 2012	FIELD	*Hymenolobium pulcherrimum*	Ducke	10
−51.45	−1.72	Tropical	Evergreen Broadleaf	Rowland et al., 2018	FIELD	*Inga alba*	(Sw.) Willd.	2
−51.45	−1.72	Tropical	Evergreen Broadleaf	Rowland et al., 2018	FIELD	*Inga capitata*	Desv.	1
−51.45	−1.72	Tropical	Evergreen Broadleaf	Rowland et al., 2018	FIELD	*Inga gracilifolia*	Ducke	2
−51.45	−1.72	Tropical	Evergreen Broadleaf	Rowland et al., 2018	FIELD	*Inga rubiginosa*	(Rich.) DC.	1
−51.45	−1.72	Tropical	Evergreen Broadleaf	Rowland et al., 2018	FIELD	*Inga vera*		2
127.53	45.38	Boreal	Deciduous Broadleaf	Yang et al., 2012	FIELD	*Juglans mandshurica*	Maxim.	41
−1.15	38.95	Temperate	Evergreen needles	Morote et al., 2021	FIELD	*Juniperus thurifera*	L.	187
116.85	42.03	Temperate	Deciduous needles	Zhao et al., 2021	FIELD	*Larix gmelinii*	(Rupr.) Kuzen.	36
117.25	42.32	Temperate	Deciduous needles	You et al., 2013	FIELD	*Larix gmelinii*	(Rupr.) Kuzen.	10
121.95	50.62	Boreal	Deciduous needles	E, 2008	FIELD	*Larix gmelinii*	(Rupr.) Kuzen.	5
124.22	52.19	Boreal	Deciduous needles	E, 2008	FIELD	*Larix gmelinii*	(Rupr.) Kuzen.	5
125.2	50.45	Boreal	Deciduous needles	E, 2008	FIELD	*Larix gmelinii*	(Rupr.) Kuzen.	5
126.63	45.72	Boreal	Deciduous needles	Wang et al., 2011	FIELD	*Larix gmelinii*	(Rupr.) Kuzen.	2
126.8	49.62	Boreal	Deciduous needles	E, 2008	FIELD	*Larix gmelinii*	(Rupr.) Kuzen.	5
127.53	45.38	Boreal	Deciduous needles	Yang et al., 2012	FIELD	*Larix gmelinii*	(Rupr.) Kuzen.	59
127.57	45.33	Boreal	Deciduous needles	Jiang et al., 2013	FIELD	*Larix gmelinii*	(Rupr.) Kuzen.	12
127.57	45.33	Boreal	Deciduous needles	Wang et al., 2003	FIELD	*Larix gmelinii*	(Rupr.) Kuzen.	61
127.67	45.4	Boreal	Deciduous needles	Dou et al., 2011	FIELD	*Larix gmelinii*	(Rupr.) Kuzen.	9
127.67	45.4	Boreal	Deciduous needles	Shi et al., 2010	FIELD	*Larix gmelinii*	(Rupr.) Kuzen.	58
127.67	45.4	Boreal	Deciduous	Xu et al., 2015	FIELD	*Larix gmelinii*	(Rupr.) Kuzen.	9

			needles					
129.42	48.67	Boreal	Deciduous needles	E, 2008	FIELD	*Larix gmelinii*	(Rupr.) Kuzen.	5
130.42	47.55	Boreal	Deciduous needles	E, 2008	FIELD	*Larix gmelinii*	(Rupr.) Kuzen.	5
−51.45	−1.72	Tropical	Evergreen Broadleaf	Rowland et al., 2018	FIELD	*Licania*	Aubl.	1
−51.45	−1.72	Tropical	Evergreen Broadleaf	Rowland et al., 2018	FIELD	*Licania membranacea*	Sagot ex Laness.	3
−51.45	−1.72	Tropical	Evergreen Broadleaf	Rowland et al., 2018	FIELD	*Licania octandra*	(Hoffmanns. ex Schult.) Kuntze	3
145.62	−17.12	Tropical	Evergreen Broadleaf	Westerband et al., 2022	LAB	*Litsea leefeana*	Merr.	1
131.11	−12.46	Tropical	Evergreen Broadleaf	Westerband et al., 2022	LAB	*Lophostemon lactifluus*	(F.Muell.) Peter G.Wilson & J.T.Waterh.	1
102.03	24.53	Temperate	Evergreen Broadleaf	Hu et al., 2010	FIELD	*Machilus bombycina*	King ex Hook.f.	30
−60.02	−3.12	Tropical	Evergreen Broadleaf	Kunert et al., 2015	FIELD	*Mangifera indica*	L.	24
117.95	26.47	Temperate	Evergreen Broadleaf	Wei et al., 2009	FIELD	*Mangifera indica*	L.	24
−79.25	−4.06	Tropical	Evergreen Broadleaf	Zach et al., 2010	FIELD	*Matayba inelegans*	Radlk.	55
−79.25	−4.06	Tropical	Evergreen Broadleaf	Zach et al., 2010	FIELD	*Miconia punctata*	(Desr.) D.Don	111
−51.45	−1.72	Tropical	Evergreen Broadleaf	Rowland et al., 2018	FIELD	*Micropholis venulosa*	Pierre	7
−51.45	−1.72	Tropical	Evergreen Broadleaf	Rowland et al., 2018	FIELD	*Minquartia guianensis*	Aubl.	6
11.5	3.38	Tropical	Evergreen Broadleaf	Meir et al., 2019	FIELD	*Musanga cecropioides*	R.Br. ex Tedlie	29
145.62	−17.12	Tropical	Evergreen Broadleaf	Westerband et al., 2022	LAB	*Myristica globosa*	(Warb.) W.J.de Wilde	1
−61.92	−10.08	Tropical	Evergreen Broadleaf	Meir et al., 2019	FIELD	*Naucleopsis krunni*		12
145.62	−17.12	Tropical	Evergreen Broadleaf	Westerband et al., 2022	LAB	*Neolitsea dealbata*	(R.Br.) Merr.	1
−51.45	−1.72	Tropical	Evergreen Broadleaf	Rowland et al., 2018	FIELD	*Newtonia suaveolens*	(Miq. Brenan)	1
172.75	−41.58	Temperate	Deciduous	Benecke, 1985	FIELD	*Nothofagus fusca*	(Colenso)	12

−51.45	−1.72	Tropical	broadleaf Evergreen Broadleaf	Rowland et al., 2018	FIELD	*Parkia ulei*	Cockayne (Harms) Kuhlm.	1
−84	10.26	Tropical	Evergreen Broadleaf	Asao et al., 2015	FIELD	*Pentaclethra macroloba*	(Willd.) Kuntze	49
131.11	−12.46	Tropical	Evergreen Broadleaf	Westerband et al., 2022	LAB	*Persoonia falcata*	R.Br.	1
151.29	−33.58	Temperate	Evergreen Broadleaf	Westerband et al., 2022	LAB	*Persoonia levis*	(Cav.) Domin	1
131.11	−12.46	Tropical	Evergreen Broadleaf	Westerband et al., 2022	LAB	*Petalostigma pubescens*	Domin	1
151.29	−33.58	Temperate	Evergreen Broadleaf	Westerband et al., 2022	LAB	*Phyllota phylicoides*	(Sieber ex DC.) Benth.	1
12.15	58.38	Boreal	Evergreen needles	Tarvainen et al., 2014	FIELD	*Picea abies*	(L.) H.Karst.	6
18.32	49.3	Boreal	Evergreen needles	Buzkova et al., 2015	FIELD	*Picea abies*	(L.) H.Karst.	132
18.53	49.5	Boreal	Evergreen needles	Acosta et al., 2008	FIELD	*Picea abies*	(L.) H.Karst.	3
18.53	49.5	Boreal	Evergreen needles	Darenova et al., 2018	FIELD	*Picea abies*	(L.) H.Karst.	13
18.53	49.5	Boreal	Evergreen needles	Janous et al., 2000	FIELD	*Picea abies*	(L.) H.Karst.	12
33	56	Boreal	Evergreen needles	Kurbatova et al., 2013	FIELD	*Picea abies*	(L.) H.Karst.	167
127.67	45.4	Boreal	Evergreen needles	Xu et al., 2015	FIELD	*Picea koraiensis*	Nakai	10
−74.43	49.69	Boreal	Evergreen needles	Hermle et al., 2010	FIELD	*Picea mariana*	Britton, Sterns & Poggenb.	6
−74.43	49.69	Boreal	Evergreen needles	Hermle et al., 2010	FIELD	*Pinus banksiana*	Lamb.	5
−27.25	28.58	Temperate	Evergreen needles	Wiser et al., 2009	FIELD	*Pinus canariensis*	C.Sm.	36
−16.57	28.3	Temperate	Evergreen needles	Brito et al., 2013	FIELD	*Pinus canariensis*	C.Sm.	41
11	47	Boreal	Evergreen needles	Wieser et al., 2004	FIELD	*Pinus cembra*	L.	142
−105.87	39.9	Temperate	Evergreen needles	Ryan, 1989	FIELD	*Pinus contorta*	Douglas ex Loudon	21
−80.58	42.66	Temperate	Evergreen needles	Kim et al., 2005	FIELD	*Pinus densiflora*	Siebold & Zucc.	1

132.65	34.38	Temperate	Evergreen needles	Kim et al., 2005	FIELD	*Pinus densiflora*	Siebold & Zucc.	131
−82.15	29.73	Temperate	Evergreen needles	Ryan et al., 1995	FIELD	*Pinus elliottii*	Engelm.	71
115.07	26.75	Temperate	Evergreen needles	Wang et al., 2018	FIELD	*Pinus elliottii*	Engelm.	34
115.07	26.75	Temperate	Evergreen needles	Wei et al., 2015	FIELD	*Pinus elliottii*	Engelm.	35
35.05	31.33	Temperate	Evergreen needles	Maseyk et al., 2008	FIELD	*Pinus halepensis*	Mill.	22
127.53	45.38	Boreal	Evergreen needles	Yang et al., 2012	FIELD	*Pinus koraiensis*	Siebold & Zucc.	50
127.67	45.4	Boreal	Evergreen needles	Dou et al., 2011	FIELD	*Pinus koraiensis*	Siebold & Zucc.	9
127.67	45.4	Boreal	Evergreen needles	Shi et al., 2010	FIELD	*Pinus koraiensis*	Siebold & Zucc.	105
127.67	45.4	Boreal	Evergreen needles	Xu et al., 2015	FIELD	*Pinus koraiensis*	Nakai	9
128.1	42.4	Temperate	Evergreen needles	Wang et al., 2005	FIELD	*Pinus koraiensis*	Siebold?&?Zucc.	56
114.04	31.49	Temperate	Evergreen needles	Chi et al., 2020	FIELD	*Pinus massoniana*	Siebold & Zucc.	14
114.07	31.82	Temperate	Evergreen needles	Yang et al., 2011	FIELD	*Pinus massoniana*	Siebold & Zucc.	8
115.07	26.75	Temperate	Evergreen needles	Wei et al., 2015	FIELD	*Pinus massoniana*	Lamb.	36
115.07	26.75	Temperate	Evergreen needles	Xu et al., 2017	FIELD	*Pinus massoniana*	Lamb.	187
−120.63	38.9	Temperate	Evergreen needles	Xu et al., 2000	FIELD	*Pinus ponderosa*	Douglas ex C.Lawson	72
−72.41	−35.5	Temperate	Evergreen needles	Bown et al., 2016	FIELD	*Pinus radiata*	D.Don	17
148.93	−35.35	Temperate	Evergreen needles	Ryan et al., 1996	FIELD	*Pinus radiata*	D.Don	5
172.75	−41.58	Temperate	Evergreen needles	Benecke, 1985	FIELD	*Pinus radiata*	D.Don	12
19.76	64.23	Boreal	Evergreen needles	Ogawa, 2006	FIELD	*Pinus sylvestris*	L.	51
30.82	62.87	Boreal	Evergreen needles	Zha et al., 2004	FIELD	*Pinus sylvestris*	L.	17
80.38	60.75	Boreal	Evergreen	Shibistova et al., 2002	FIELD	*Pinus sylvestris*	L.	11

			needles					
127.67	45.4	Boreal	Evergreen needles	Xu et al., 2015	FIELD	*Pinus sylvestris*		11
114.04	31.49	Temperate	Evergreen needles	Chi et al., 2020	FIELD	*Pinus taeda*	L.	20
114.07	31.82	Temperate	Evergreen needles	Yang et al., 2011	FIELD	*Pinus taeda*	L.	13
131.11	−12.46	Tropical	Evergreen Broadleaf	Westerband et al., 2022	LAB	*Planchonia careya*	(F.Muell.) R.Knuth	1
145.62	−17.12	Tropical	Evergreen Broadleaf	Westerband et al., 2022	LAB	*Polyscias australiana*	(F.Muell.) Philipson	1
101.27	21.93	Temperate	Evergreen Broadleaf	Yan et al., 2009	FIELD	*Pometia tomentosa*		24
114.5	36.42	Temperate	Deciduous Broadleaf	Zhang et al., 2019	FIELD	*Populus davidiana*	Carrière	16
127.67	45.4	Boreal	Deciduous broadleaf	Dou et al., 2011	FIELD	*Populus davidiana*	Dode	9
114.5	36.42	Temperate	Deciduous broadleaf	Liu et al., 2019	FIELD	*Populus tomentosa*	Carrière	30
127.53	45.38	Boreal	Deciduous Broadleaf	Yang et al., 2012	FIELD	*Populus tremula*	Dode	41
−106.2	53.63	Boreal	Deciduous broadleaf	Gaumont et al., 2006	FIELD	*Populus tremuloides*	Michx.	16
−51.45	−1.72	Tropical	Evergreen Broadleaf	Rowland et al., 2018	FIELD	*Pouteria anomala*	(Pires) T.D.Penn.	5
−51.45	−1.72	Tropical	Evergreen Broadleaf	Rowland et al., 2018	FIELD	*Pouteria cladantha*	Sandwith	1
−51.45	−1.72	Tropical	Evergreen Broadleaf	Rowland et al., 2018	FIELD	*Pouteria decorticans*	T.D.Penn.	6
−51.45	−1.72	Tropical	Evergreen Broadleaf	Rowland et al., 2018	FIELD	*Pouteria gongrijpii*	Eyma	1
−51.45	−1.72	Tropical	Evergreen Broadleaf	Rowland et al., 2018	FIELD	*Pouteria guianensis*	Griseb.	1
−51.45	−1.72	Tropical	Evergreen Broadleaf	Rowland et al., 2018	FIELD	*Pouteria trilocularis*	Cronquist	1
−51.45	−1.72	Tropical	Evergreen Broadleaf	Rowland et al., 2018	FIELD	*Prieurella prieurii*	(A.DC.)?Aubré v.	1
−51.45	−1.72	Tropical	Evergreen Broadleaf	Rowland et al., 2018	FIELD	*Protium paniculatum*	Engl.	1
−51.45	−1.72	Tropical	Evergreen Broadleaf	Rowland et al., 2018	FIELD	*Protium pilosissimum*	Swart	1

−51.45	−1.72	Tropical	Evergreen Broadleaf	Rowland et al., 2018	FIELD	*Protium tenuifolium*	(Engl.) Engl.	4
145.62	−17.12	Tropical	Evergreen Broadleaf	Westerband et al., 2022	LAB	*Pseudoweinmannia lachnocarpa*	(F.Muell.) Engl.	1
145.62	−17.12	Tropical	Evergreen Broadleaf	Westerband et al., 2022	LAB	*Pullea stutzeri*	(F.Muell.) Gibbs	1
−51.45	−1.72	Tropical	Evergreen Broadleaf	Rowland et al., 2018	FIELD	*Qualea paraensis*	Ducke	1
114.04	31.49	Temperate	Deciduous broadleaf	Chi et al., 2020	FIELD	*Quercus acutissima*	Carruth.	24
114.07	31.82	Temperate	Deciduous Broadleaf	Yang et al., 2011	FIELD	*Quercus acutissima*	Carruth.	15
3.58	43.73	Temperate	Deciduous Broadleaf	Rodriguez-Calcerrada et al., 2014	FIELD	*Quercus ilex*	L.	29
127.53	45.38	Boreal	Deciduous Broadleaf	Yang et al., 2012	FIELD	*Quercus mongolica*	Fisch. ex Turcz.	55
128.1	42.4	Temperate	Deciduous broadleaf	Wang et al., 2005	FIELD	*Quercus mongolica*	Fisch. ex Turcz.	55
−4.02	40.87	Temperate	Deciduous broadleaf	Salomon et al., 2016	FIELD	*Quercus pyrenaica*	Willd.	9
−75.17	42.5	Temperate	Deciduous Broadleaf	Reinmann et al., 2015	FIELD	*Quercus rubra*	L.	20
145.62	−17.12	Tropical	Evergreen Broadleaf	Westerband et al., 2022	LAB	*Racosperma celsum*	Tindale	1
145.62	−17.12	Tropical	Evergreen Broadleaf	Westerband et al., 2022	LAB	*Rapanea porosa*	F.Muell.	1
132.65	34.38	Temperate	Deciduous Broadleaf	Kim et al., 2006	FIELD	*Robinia pseudoacacia*	L.	70
145.62	−17.12	Tropical	Evergreen Broadleaf	Westerband et al., 2022	LAB	*Rockinghamia angustifolia*	(Benth.) Airy Shaw	1
116.33	40.03	Temperate	Deciduous Broadleaf	Han et al., 2015	FIELD	*Salix matsudana*	Koidz.	26
102.03	24.53	Temperate	Evergreen Broadleaf	Hu et al., 2010	FIELD	*Schima noronhae*	Reinw. ex Blume	30
113.28	23.13	Temperate	Evergreen Broadleaf	Zhu et al., 2009	FIELD	*Schima superba*	Gardner & Champ.	72
−51.45	−1.72	Tropical	Evergreen Broadleaf	Rowland et al., 2018	FIELD	*Sclerolobium paraense*	Huber	1
−60.02	−3.12	Tropical	Evergreen Broadleaf	Kunert, 2018	FIELD	*Scleronema micranthum*	(Ducke) Ducke	14
114.03	4.2	Tropical	Evergreen	Katayama et al., 2014	FIELD	*Shorea beccariana*	(Burck)	3

			Broadleaf				P.S.Ashton & J.Heck.	
151.29	−33.58	Temperate	Evergreen Broadleaf	Westerband et al., 2022	LAB	*Solanum aviculare*	G.Forst.	1
145.62	−17.12	Tropical	Evergreen Broadleaf	Westerband et al., 2022	LAB	*Steganthera laxiflora*	(Benth.) Whiffin & Foreman	1
−51.45	−1.72	Tropical	Evergreen Broadleaf	Rowland et al., 2018	FIELD	*Stryphnodendron*	Mart.	1
116.33	40.03	Temperate	Deciduous Broadleaf	Han et al., 2015	FIELD	*Styphnolobium japonicum*	L.	5
−51.45	−1.72	Tropical	Evergreen Broadleaf	Rowland et al., 2018	FIELD	*Swartzia*	Bird.	1
−51.45	−1.72	Tropical	Evergreen Broadleaf	Rowland et al., 2018	FIELD	*Swartzia racemosa*	Benth.	7
151.29	−33.58	Temperate	Evergreen Broadleaf	Westerband et al., 2022	LAB	*Syncarpia glomulifera*	(Sm.) Nied.	1
−51.45	−1.72	Tropical	Evergreen Broadleaf	Rowland et al., 2018	FIELD	*Syzygiopsis oppositifolia*	Ducke	8
131.11	−12.46	Tropical	Evergreen Broadleaf	Westerband et al., 2022	LAB	*Terminalia ferdinandiana*	Exell	1
127.53	45.38	Boreal	Deciduous Broadleaf	Yang et al., 2012	FIELD	*Tilia amurensis*	Rupr.	36
128.1	42.4	Temperate	Deciduous broadleaf	Wang et al., 2005	FIELD	*Tilia amurensis*	Rupr.	45
127.53	45.38	Boreal	Deciduous Broadleaf	Yang et al., 2012	FIELD	*Ulmus davidiana*	Koidz.	54
−51.45	−1.72	Tropical	Evergreen Broadleaf	Rowland et al., 2018	FIELD	*Vantanea parviflora*	Lam.	1
−51.45	−1.72	Tropical	Evergreen Broadleaf	Rowland et al., 2018	FIELD	*Vatairea erythrocarpa*	(Ducke) Ducke	1
−84	10.26	Tropical	Evergreen Broadleaf	Asao et al., 2015	FIELD	*Virola koschnyi*	Warb.	37
−61.92	−10.08	Tropical	Evergreen Broadleaf	Meir et al., 2019	FIELD	*Virola michelii*	Heckel	16
−51.45	−1.72	Tropical	Evergreen Broadleaf	Rowland et al., 2018	FIELD	*Virola michelii*	Heckel	2
−84	10.26	Tropical	Evergreen Broadleaf	Asao et al., 2015	FIELD	*Vochysia guatemalensis*	Donn.Sm.	42
−51.45	−1.72	Tropical	Evergreen Broadleaf	Rowland et al., 2018	FIELD	*Vouacapoua americana*	Aubl.	9

131.11	−12.46	Tropical	Evergreen Broadleaf	Westerband et al., 2022	LAB	*Xanthostemon paradoxus*	F.Muell.	1
−98.75	55.75	Temperate	Evergreen needles	Lavigne and Ryan, 1997	FIELD	*Picea mariana*	Britton, Sterns & Poggenb.	1064
−98.75	55.75	Temperate	Evergreen needles	Lavigne and Ryan, 1997	FIELD	*Pinus banksiana*	Lamb.	1788
−98.75	55.75	Temperate	Deciduous Broadleaf	Lavigne and Ryan, 1997	FIELD	*Populus tremuloides*	Michx.	1303

table S2. Detailed information of stem respiration data. This table shows the detailed information of stem respiration data as a sub-dataset of GSRD used in this work. The table includes the following attributes: LON and LAT, representing latitude and longitude of sites. CLIMATE ZONE represents the climate zone of each site (including Tropical, Temporal (between latitude 20 and 45º), and Boreal (above latitude 45º)). PFT represents plant functional types, and REF represents the literature from which the data is sourced, MEAS stands for measurement method, some measurements were made in the field (FIELD) and some in the laboratory (LAB). FINAL_SNPNAME represents the calibrated species name and includes AUTHORITY information. OBS NUM is the number of samples of a particular species per site. The list is presented based on the species name, grouped alphabetically, except for the last three rows which are temporal data from the same site. Please refer to the attached Dataset for detailed data.

Quantity	Theory prediction	Fixed effects			Random effects		R^2	df
		Fitted coefficient	p	Intercept (mean ± SE)	Measurement Methods (Variance ± SD)	Residual (Variance ± SD)		
r_{s25}	−0.101	−0.097± 0.002	<0.001	1.15 ± 0.50	−0.49 ± 0.70	−0.52 ± 0.72	0.57	4625
$r_{s.gt}$	−0.023	−0.018± 0.002	<0.001	−0.82 ± 0.50	−0.49 ± 0.70	−0.52 ± 0.72	0.49	4625

table S3. Global trends of stem respiration in relation to temperature. Statistical output using the global dataset shown in Figure 1. r_{s25} represents stem respiration standardized to the reference temperature of 25 ℃; $r_{s.gt}$ represents stem respiration standardized to the mean growing temperature. Mixed-effect model was performed for all data considering different measuring methods as a random effect. The table provides confidence intervals, R-squared values (R^2), p-values (p), and degrees of freedom (df) associated with each regression model.

	Df	Sum Sq	Mean Sq	F value	Pr (>F)
Measurement Methods	1	26	25.741	36.31	<1.8e−09***
Residuals	4625	3279	0.709		

table S4. ANOVA result of field and laboratory stem respiration. The analysis of variance tests the differences between two sets of data using measurement methods as the distinguishing dimension, one set being in the field and the other set being in the lab.

Signif. codes: 0 '***'

Quantity	Theoretical prediction	fitted coefficient	confidence intervals		Intercept (mean ± SE)	R^2	p	df
			2.50%	97.50%				
r_{s25}	−0.101	−0.081	−0.098	−0.063	−0.48 ± 0.21	.33	<0.001	64
$r_{s.gt}$	−0.023	−0.002	−0.020	0.016	−1.94 ± 0.21		>0.5	64

table S5. Global trends of site-mean stem respiration to temperature. Statistical output from regression analysis using the data shown in fig.S2. r_{s25} represents stem respiration standardized to the reference temperature of 25 °C; $r_{s.gt}$ represents stem respiration standardized to the mean growing temperature. All data was analyzed by linear regression analysis using base R, considering different measuring methods as an influencing factor. The table provides confidence intervals, R-squared values (R^2), p-values (p), and degrees of freedom (df) associated with regression model.

Quantity	Prediction	fitted coefficient	confidence intervals		Intercept (mean ± SE)	R^2	p	df
			2.50%	97.50%				
Individual r_s		–0.154	−0.161	−0.148	1.44 ± 0.12	0.55	<0.001	516
	–0.101							
Site-mean r_s		–0.101	−0.139	−0.063	0.95 ± 0.53	0.43	<0.05	10

table S6. Global trends of stem respiration without temperature standardization in relation to temperature. Statistical output from EIV (Errors-in-Variables) regression analysis using the data shown in fig.S3. r_s represents stem respiration whose measuring temperature was 1℃ within 25℃. Individual r_s represents raw data, while site-mean r_s represents mean r_s value within each bin after dividing T_5 into 20 bins. The table provides confidence intervals, R-squared values (R^2), p-values (p), and degrees of freedom (df) associated with regression model.

Model	T_g	ln E	Slope of T_g (mean ± se)	Slope of ln E (mean ± se)	R^2	RMSE	VIF	AIC
$\ln r_{s25} \sim T_{g6} + \ln E_{13}$	6	13	−0.106 ± 0.005	1.038 ± 0.018	0.49	2.37	2.01	8201
$\ln r_{s25} \sim T_{g6} + \ln E_{12}$	6	12	−0.107 ± 0.005	1.019 ± 0.018	0.49	2.37	2.03	8211
$\ln r_{s25} \sim T_{g7} + \ln E_{14}$	7	14	−0.124 ± 0.006	1.131 ± 0.021	0.50	2.37	2.52	8187
$\ln r_{s25} \sim T_{g7} + \ln E_{13}$	7	13	−0.127 ± 0.006	1.117 ± 0.020	0.50	2.37	2.54	8156
$\ln r_{s25} \sim T_{g7} + \ln E_{12}$	7	12	−0.127 ± 0.006	1.095 ± 0.020	0.50	2.37	2.56	8171
$\ln r_{s25} \sim T_{g7} + \ln E_{11}$	7	11	−0.125 ± 0.006	1.064 ± 0.020	0.49	2.37	2.56	8225
$\ln r_{s25} \sim T_{g8} + \ln E_{14}$	8	14	−0.139 ± 0.006	1.196 ± 0.023	0.50	2.37	3.07	8170
$\ln r_{s25} \sim T_{g8} + \ln E_{12}$	8	12	−0.139 ± 0.006	1.149 ± 0.022	0.50	2.37	3.08	8171
$\ln r_{s25} \sim T_{g8} + \ln E_{13}$	8	13	−0.141 ± 0.006	1.178 ± 0.022	0.50	2.37	3.08	8145
$\ln r_{s25} \sim T_{g9} + \ln E_{13}$	9	13	−0.137 ± 0.006	1.185 ± 0.024	0.49	2.37	3.59	8229

table S7. Multiple regression analysis of different time-scale combinations of transpiration and temperature in relation to stem respiration. Multiple regression analysis between natural log-transformed r_{s25} and temperature and natural log-transformed transpiration. r_{s25} represents stem respiration standardized to the reference temperature of 25 ℃. Growth temperature (T_g) and Transpiration (E) are an average of different time scales of days before measurement (the second and third columns in the table represent different time scales). The table provides confidence intervals, R-squared values (R^2), p-values (p), and degrees of freedom (df) Root Mean Square Deviation (RMSE), Variance Inflation Factors (VIF) and Akaike information criterion (AIC) associated with each regression model.

Species	Theoretical prediction	fitted coefficient	confidence intervals		Intercept (mean ± SE)	R^2	p	df
			2.50%	97.50%				
B.alleghaniensis		−0.096	−0.135	−0.058	5.37 ± 0.95	.40	<0.001	9
P. nigra		−0.054	−0.071	−0.037	3.59 ± 0.41	.44	<0.001	13
P. pinaster		−0.123	−0.157	−0.090	6.04 ± 0.91	.49	<0.001	14
	−0.101							
P. pinea		−0.271	−0.384	−0.158	9.23 ± 2.68	.49	0.05	6
P. sylvestris		−0.135	−0.164	−0.106	6.12 ± 0.79	.65	<0.001	12
All species		−0.106	−0.122	−0.089	5.32 ± 0.42	.44	<0.001	54

table S8. Mathematical details of each species in a warming experiment. Statistical output from linear regression analysis using the data shown in Fig. 3. r_{s25} represents stem respiration standardized to the reference temperature of 25 °C. The table provides confidence intervals, R-squared values (R^2), p-values (p), and degrees of freedom (df) associated with each regression model.

Prediction	fitted coefficient	confidence intervals		R^2	p	df
		2.50%	97.50%			
–0.101	–0.084	−0.089	−0.080	.23	<0.001	1240

table S9. Global trends of stem respiration to temperature based on measurements of *Pinus*. Statistical output from EIV (Errors-in-Variables) regression analysis using the data shown in fig.S4. r_{s25} represents stem respiration standardized to the reference temperature of 25 °C. The table provides confidence intervals, R-squared values (R^2), p-values (p), and degrees of freedom (df).

	Estimate	Std.Error	p	df
Intercept	0.533	0.035	<0.001	517

table S10. Parameter calibration of the stem respiration model. The calibration was based on samples measured at temperatures of 25±1℃ from the Global Stem Respiration Dataset. The linear regression used a fixed slope of −0.1 (theoretical predicted value) to estimate the intercept and its standard error, representing the parameter's uncertainty. The table provides intercept, standard error of intercept (se), p-values (p), and degrees of freedom (df) associated with regression model.

Q_{10}	Theoretical Prediction	Fitted slope between r_{s25} and T_5	R^2	p
1.6	−0.070	−0.077 (se=0.003)	0.17	<0.001
1.8	−0.081	−0.085 (se=0.003)	0.20	<0.001
2.0	−0.092	−0.091 (se=0.003)	0.23	<0.001
2.2	−0.101	−0.098 (se=0.003)	0.26	<0.001
2.4	−0.110	−0.103 (se=0.003)	0.28	<0.001
2.6	−0.118	−0.108 (se=0.003)	0.29	<0.001

table S11. Validating stability with varying Q_{10} parameter values. Theoretical prediction and fitted slope between r_{s25} and T_5 of various Q_{10} values. r_{s25} represents stem respiration standardized to the reference temperature of 25 ℃ using different values of Q_{10} following fixed-Q_{10} equation. Error in Variables regression analysis (EIV) was performed for all data together including data from field measurements and lab ones. The table provides standard error (within parentheses), R-squared values (R^2) and p-values (p), associated with each regression model.

Quantity	Theoretical Prediction	fitted coefficient	confidence intervals		Intercept (mean ± SE)	R^2	p	df
			2.50%	97.50%				
T_5	−0.101	−0.106	−0.109	−0.103	1.10 ± 0.04	0.32	<0.001	4543
D		−0.013	−0.014	−0.013				

table S13. Mathematical details of multiple regression analysis of r_{s25} with tree trunk diameter and T_5. r_{s25} represents the "in field" measurements on stem respiration standardized to the reference temperature of 25 °C. D represents diameters from stem samples with stem respiration measurements, T_5 is the mean value of the excess temperature above 5°C. Error in Variables regression analysis (EIV) was performed for all data together. The table provides confidence intervals, R-squared values (R^2), p-values (p), and degrees of freedom (df).

Quantity	Theoretical prediction	Measurements	Fitted coefficient	Confidence intervals		Intercept (mean ± SE)	R^2	p	df
				2.50%	97.50%				
r_{s25}	−0.101	Angiosperms	−0.092	−0.095	−0.088	1.88 ± 0.05	0.23	<0.001	2425
		Gymnosperms	−0.084	−0.088	−0.079	3.22 ± 0.04	0.17	<0.001	2117
		In lab	−0.110	−0.143	−0.078	3.27 ± 0.57	0.27	<0.01	79
		All data	−0.090	−0.093	−0.087	1.85 ± 0.04	0.64	<0.001	4625

table S14. Global trends of stem respiration (parenchyma mass-based) at reference temperature (r_{s25}) in relation to the mean value of the excess temperature above 5℃ (T_5). r_{s25} represents parenchyma mass-based stem respiration standardized to the reference temperature of 25 ℃. Error in Variables regression analysis (EIV) was performed for angiosperms, gymnosperms and lab data separately. We usded Linear Mixed Models (LMM) for all data considering different group or measurements as random effects. The table provides confidence intervals, R-squared values (R^2), p-values (p), and degrees of freedom (df) associated with each regression model.

Quantity	Theoretical prediction	fitted coefficient	confidence intervals		Intercept (mean ± SE)	R^2	p	df
			2.50%	97.50%				
lnVPD	0.536	0.130	0.0931	0.167	−0.310 ± 0.19	0.253	<0.001	4823
T_5	−0.100	−0.142	−0.0253	0.0165				

table S15. Mathematical details of multiple regression analysis between r_{s25} and *VPD*, T_5. Statistical output from a multiple regression analysis using the data shown in fig. S9. r_{s25} represents stem respiration standardized to the reference temperature of 25 ℃. *VPD* is vapor pressure deficit (Pa) at a given site and T_5 (℃) is the mean value of the excess temperature above 5℃. The table provides confidence intervals, R-squared values (R^2), p-values (p), and degrees of freedom (df) associated with each regression model.